How gas flow design can influence the performance of a DBD plasma reactor for dry reforming of methane

How gas flow design can influence the performance of a DBD plasma reactor for dry reforming of methane.

Y. Uytdenhouwen [a,b], J. Hereijgers [c], T. Breugelmans [c,d], P. Cool [b], A. Bogaerts [a*]

[a] Research Group PLASMANT, Department of Chemistry, University of Antwerp, Universiteitsplein 1, 2610 Wilrijk, Belgium

[b] Research group LADCA, Department of Chemistry, University of Antwerp, Universiteitsplein 1, 2610 Wilrijk, Belgium

[c] Research group Applied Electrochemistry & Catalysis, University of Antwerp, Universiteitsplein 1, 2610 Wilrijk, Belgium

[d] Separation & Conversion Technologies, VITO, Boeretang 200, 2400 Mol, Belgium

*Corresponding author:
Annemie Bogaerts
Universiteitsplein 1, B2.09
Wilrijk B-2610, Belgium
+3232652377
annemie.bogaerts@uantwerpen.be

Keywords:
Plasma; Dielectric barrier discharge; Dry reforming of methane; Flow pattern; Mixing pattern; Reactor design

Abbreviation:
VOC, Volatile organic compounds; NOx, Nitrogen oxides; DRM, Dry reforming of methane; DBD, Dielectric barrier discharge; SOEC, Solid oxide electrolyzer cell; PMMA, Poly(methyl methacrylate); POM, Polyoxymethylene; SEI, Specific energy input; PSD, Power surface density; P, Power; n, Number of consecutive periods; T, Period; U, Voltage; I, Current; t, Time;TCD, GC, Gas chromatograph; Thermal conductivity detector; FID, Flame ionization detector; TCD, Thermal conductivity detector; X, Conversion; $\dot{y}$, Molar flow rate of component y; X_{Total}, Total conversion; EC, Energy cost; $\dot{V}$, Volumetric flow rate; V_m, Molar volume; S_n, Sample standard deviation; $T(p,n_s)$, Student's t-distribution for sample size n_s and probability p set at 95%; CFD, Computational fluid dynamics; RTD, Residence time distribution; MS, Mass spectrometer

1

Abstract

DBD plasma reactors are commonly used in a static 'one inlet – one outlet' design that goes against reactor design principles for multi-component reactions, such as dry reforming of methane (DRM). Therefore, in this paper we have developed a novel reactor design, and investigated how the shape and size of the reaction zone, as well as gradual gas addition, and the method of mixing CO_2 and CH_4 can influence the conversion and product composition of DRM. Even in the standard 'one inlet – one outlet' design, the direction of the gas flow (i.e. short or long path through the reactor, which defines the gas velocity at fixed residence time), as well as the dimensions of the reaction zone and the power delivery to the reactor, largely affect the performance. Using gradual gas addition and separate plasma activation zones for the individual gases give increased conversions within the same operational parameters, by optimising mixing ratios and kinetics. The choice of the main (pre-activated) gas and the direction of gas flow largely affect the conversion and energy cost, while the gas inlet position during separate addition only influences the product distribution.

2

1 Introduction

Plasma reactors have been of interest for challenging environmental and sustainable chemistry applications, such as volatile organic compounds (VOCs) destruction [1,2], N_2 fixation into ammonia or NOx [3], and greenhouse gas conversion (e.g. CO_2 dissociation and dry reforming of methane (DRM)) [4]. These reactors offer an energy-rich, reactive environment at yet relatively mild conditions, i.e. ambient temperature and pressure, to perform the aforementioned reactions. This will result in shorter steady-state times, giving us the possibility of quick on-and-off-switching, of interest for coupling with fluctuating renewable electricity [5], because less heat is dissipated in the reactor.

One of the most studied plasma reactors for gas conversion reactions is the dielectric barrier discharge (DBD) reactor due to its robustness, reliable operation under variable conditions, and scalability [6]. Optimization efforts for this reactor are mainly focussed on adding a (catalytic) packing material to the reaction volume, reducing the discharge gap to smaller dimensions, and/or pulsing the applied power, with mixed results for their influence on conversion, selectivity, and energy efficiency [7–18]. During these types of investigations, little creative engineering is done besides such optimizations, i.e. the DBD reactor (in either parallel plate or co-axial design, with or without packing) is virtually always used in a static 'one inlet – one outlet' design.

While this is not really an issue with a single-gas inlet stream, it is known from reaction engineering that such a design is rarely the best configuration for multi-gas inlet streams [19]. It can lead to reactor operation at non-ideal kinetic conditions, resulting in improper conversions of one or more of the reagents, e.g. more CH_4 conversion than the more desired CO_2 conversion in DRM (see table 1 from Michielsen et al. [16]) or "optimal conversions" at stoichiometric unfavourable ratios, e.g. optimal NH_3 conversions at $H_2 : N_2$ ratios (far) below 1 instead of 3 [17,20–23]. This non-ideal behaviour of multi-gas reactions could be resolved by

3

correct reactor design, such as the size or type of reactor (batch, continuous stirring tank, plug-flow, or combined "real" reactor), reactors in series and/or parallel, recycling, and/or separate addition of reactants [19].

Few researchers have tried innovative solutions and alterations to the traditional DBD reactor design in an attempt to optimize its performance. Examples are a fluidized (catalytic) bed [24], forcing the gas flow through a thin walled porous (catalytic) tube [20,25], a sintered metal fibre (catalytic) electrode for product draining [26], a combined AC/DC DBD reactor for honeycomb structures [27], and a DBD reactor combined with a solid oxide electrolyzer cell (SOEC) [28]. Although (significant) improvements were reported in these investigations, they still applied a 'one inlet – one outlet' design. To our knowledge, only Huang and co-workers took a new approach by designing a Y-shaped reactor, allowing separate addition of CO_2 and CH_4 for DRM [29,30]. This design allowed them to pre-activate one or both of the individual gases before mixing them together as excited species, showing enhanced conversion and energy efficiency. Moreover, even this separate plasma activation was able to produce hydrocarbons, and plasma activation of only one of the gases could react with unactivated gas. Based on these findings and the knowledge from traditional reactor engineering, we believe that a lot of improvements can still be expected, in terms of the design of DBD reactors for multi-gas reactions.

Therefore, in this work, we investigate how the performance of a DBD reactor can be improved by changing the way in which CO_2 and CH_4 are added to, and mixed in, the reactor. We designed a new multi inlet/outlet parallel plate DBD reactor that allows us to quickly change the geometry of the reaction volume, in order to accommodate a multitude of different flow and mixing patterns. We will elucidate how electrode length, different gas ratios, gradual gas addition, and separate plasma activation zones for the individual gases will influence the reactor performance compared to the standard 'one inlet – one outlet' design.

4

2 Methods and theory

2.1 Novel multi-purpose DBD reactor

We designed and built (CNC mill, Isel Euromod MP45) a new DBD reactor with maximum adaptability in mind, as shown in Figure 1. The parallel plate design was chosen over the more popular co-axial design because the ceramic dielectric tubes of the latter (typically glass, quartz, or alumina) require a lot of intricate and expensive work to change the geometry, and to add for example side inlets/outlets. Our design allows us to modify only one plastic 'spacer' layer, which is easy and cheap to manufacture (along with the corresponding gas connections), in order to change the entire gas flow and mixing pattern in the reactor.
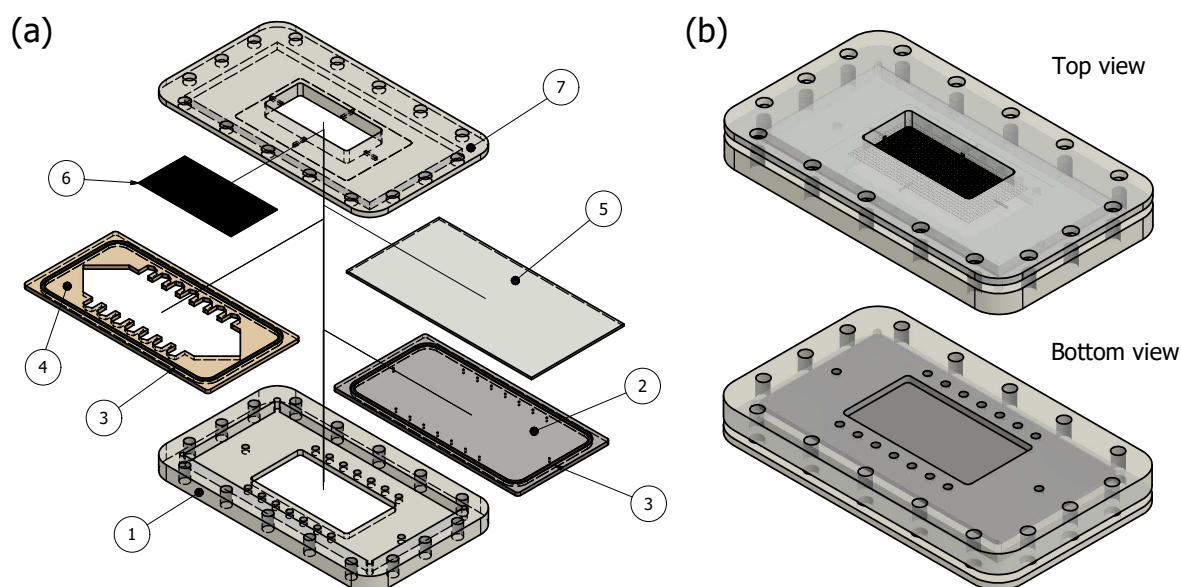

Figure 1: (a) Expanded view and (b) assembled views of the novel parallel plate DBD reactor design used in this work, comprised of PMMA holders (1 and 7), a grounded aluminium electrode (2), O-rings (3), POM spacer (4), borosilicate glass dielectric (5), and high voltage stainless steel mesh electrode (6).

The main body of the reactor consists of a PMMA 'bottom holder' (1) that holds all components of the DBD reactor together. It features a rectangular access hole to allow grounding of the grounded electrode (2), 14 small holes to pass-through any number of desired gas connections to the grounded electrode (2), and 16 threaded holes to receive M5 bolts. The grounded aluminium electrode (2) (200x100x3.5 mm) is added to the bottom holder, which features 14
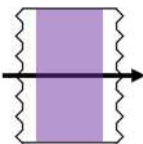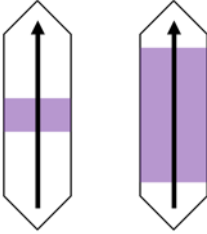
¼"-28 UNF threaded 3 mm deep holes on the bottom side to receive the desired number of gas connections (XP-330X flangeless nuts, IDEX), 14 1 mm holes on the top side to pass-through the gas, and a 2 mm deep cut groove around the edges to accommodate a 3 mm thick O-ring (3). A POM 'spacer' layer (4) (200x100x3.5 mm) is added on top of the grounded electrode. By changing the inner shape of the spacer, we can shape and define the geometry of the reaction volume. This layer also has a groove and O-ring (3). A sheet of borosilicate glass (5) (200x100x2.25 mm) (Borofloat, Glasatelier Saillaert) and a stainless steel mesh (6) (100x50 mm) were added on top of the spacer to complete the DBD configuration. Finally, a PMMA 'top holder' was added on top of the entire layer stack, featuring a rectangular access hole to connect the stainless steel mesh to the high voltage, and 16 5 mm holes around the edge of the holder to bolt everything airtight with 16 M5 bolts.
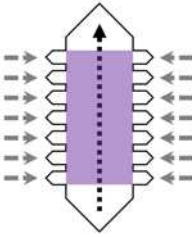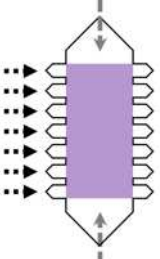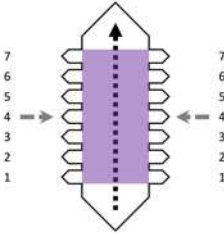
2.2 Reactor configurations
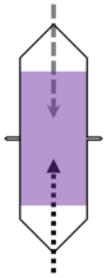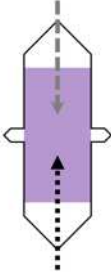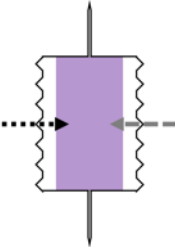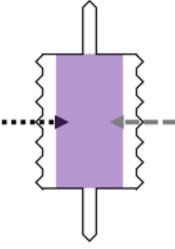
Different configurations have been tested in this work. Table 1 summarizes all configurations with the abbreviation, a short description, a schematic picture, and the conditions being used.

The standard operating conditions used in this work are a total flow rate of 50 mL/min consisting of a 1:1 CO_2 : CH_4 ratio, performed at 30 W (3 kHz) and 1 bar, a spacer thickness of 3.5 mm, and a 100x50 mm high-voltage electrode. This results in an residence time of 21 s, a specific energy input (SEI) of 36 J/mL (or 8.36 eV/molecule), and a power surface density (PSD) of 0.6 W/cm^2. Variations to these parameters for the individual configurations will be listed in the results section.

6

Table 1: Different configurations used in this work with the associated abbreviation, short description, and schematic picture.

Configuration	Abbreviation	Description	Schematic picture	Conditions
Long (Benchmark)	L	Traditional long 'one inlet – one outlet' design, 1:1 DRM mixture fed through the bottom hole and exit via the top hole. This configuration acts as the benchmark for our results. Performed at standard conditions.		$P = 30$ W $\dot{V}_t = 50$ mL/min $\dot{V}_{CO_2} = 25$ mL/min $\dot{V}_{CH_4} = 25$ mL/min
Short	S	Traditional 'one inlet – one outlet' design, but gas flow 90° shifted, 1:1 DRM mixture fed through the 7 left side holes and exit via the 7 right side holes. This configuration evaluates the influence of a narrow vs wide geometry, while keeping the same residence time as in the long reactor. Performed at standard conditions.		$P = 30$ W $\dot{V}_t = 50$ mL/min $\dot{V}_{CO_2} = 25$ mL/min $\dot{V}_{CH_4} = 25$ mL/min
Electrode length	25 50 75 100 (L)	Traditional long 'one inlet – one outlet' design, 1:1 DRM mixture fed through the bottom hole and exit via the top hole. The electrode length is varied by replacing the standard high-voltage electrode of the long reactor (100 mm) with electrode lengths between 25 and 75 mm.		P = variable $\dot{V}_t$ = variable $\dot{V}_{CO_2} = \frac{\dot{V}_t}{2}$ mL/min $\dot{V}_{CH_4} = \frac{\dot{V}_t}{2}$ mL/min
CO_2 : CH_4 ratio	1:0 6:1 3:1 1:1 (L) 1:3 1:6 0:1	Traditional long 'one inlet – one outlet' design, in which different gas mixing ratios are fed through the bottom hole and exit via the top hole. This configuration evaluates how different ratios show different conversions, because non-equimolar mixing will occur in the next configurations. Note that the 1:1 ratio is the same result as in the L configuration.		$P = 30$ W $\dot{V}_t = 50$ mL/min $\dot{V}_{CO_2}$ = variable $\dot{V}_{CH_4}$ = variable

Long with gradual addition	LGA	Long reactor where the main gas (either CO_2 or CH_4; black arrow) enters from the bottom hole, with gradual addition of the secondary gas (grey arrows) through the 14 side inlets, and one combined exit at the top hole. This configuration allows for a constant addition of unreacted secondary gas. Performed at standard conditions; each side inlet thus receives a 14th of the individual flow rate.		$P = 30$ W $\dot{V}_t = 50$ mL/min $\dot{V}_{CO_2} = 25$ mL/min $\dot{V}_{CH_4} = 25$ mL/min
Short with gradual addition	SGA	Short reactor where the main gas (either CO_2 or CH_4; black arrows) enters from the left 7 side holes, with gradual addition of the secondary gas through the top and bottom inlets (grey arrows), and one combined outlet stream via the 7 right side holes. Performed at standard conditions; each side inlet thus receives a 7th of the individual flow rate and the top and bottom inlet receive half the individual flow rate. (similar to LGA but 90° shifted)		$P = 30$ W $\dot{V}_t = 50$ mL/min $\dot{V}_{CO_2} = 25$ mL/min $\dot{V}_{CH_4} = 25$ mL/min
Long with one side addition	1 2 3 4 5 6 7	Long reactor where the main gas (either CO_2 or CH_4) enters from the bottom hole, with side addition of the secondary gas through one of the 7 side inlet pairs (hence, always two at the same time), and one combined exit at the top hole. Early addition will show similar behaviour as the benchmark, while a delay of the secondary gas allows pre-activation of the main gas by the plasma. All positions for the side addition are tested individually, with the bottom side pair being "inlet 1" and the top side pair being "inlet 7". Performed at standard conditions; each side inlet being used thus receives half the individual flow rate.		$P = 30$ W $\dot{V}_t = 50$ mL/min $\dot{V}_{CO_2} = 25$ mL/min $\dot{V}_{CH_4} = 25$ mL/min

Long with separate addition and narrow side outlets	LSN	Long reactor where one gas (either CO_2 or CH_4) enters via the top inlet and the other gas via the bottom inlet. The gases are allowed to react individually before mixing in the middle and exiting via two narrow side outlets (one at each side). Performed at standard conditions.		$P = 30$ W $\dot{V}_t = 50$ mL/min $\dot{V}_{CO_2} = 25$ mL/min $\dot{V}_{CH_4} = 25$ mL/min
Long with separate addition and wide side outlets	LSW	Long reactor where one gas (either CO_2 or CH_4) enters via the top inlet and the other gas via the bottom inlet. The gases are allowed to react individually before mixing in the middle and exiting via two wider side outlets (one at each side). Performed at standard conditions.		$P = 30$ W $\dot{V}_t = 50$ mL/min $\dot{V}_{CO_2} = 25$ mL/min $\dot{V}_{CH_4} = 25$ mL/min
Short with separate addition and narrow side outlets	SSN	Short reactor where one gas (either CO_2 or CH_4) enters via the 7 left inlets and the other gas via the 7 right inlets. The gases are allowed to react individually before mixing in the middle and exiting via narrow top and bottom outlets. Performed at standard conditions.		$P = 30$ W $\dot{V}_t = 50$ mL/min $\dot{V}_{CO_2} = 25$ mL/min $\dot{V}_{CH_4} = 25$ mL/min
Short with separate addition and wide side outlets	SSW	Short reactor where one gas (either CO_2 or CH_4) enters via the 7 left inlets and the other gas via the 7 right inlets. The gases are allowed to react individually before mixing in the middle and exiting via wider top and bottom outlets. Performed at standard conditions.		$P = 30$ W $\dot{V}_t = 50$ mL/min $\dot{V}_{CO_2} = 25$ mL/min $\dot{V}_{CH_4} = 25$ mL/min

2.3   Experimental set-up

For each experiment, the reactor was placed in the experimental set-up shown in Figure 2. The high voltage was supplied by a high-voltage amplifier (TREK, Model 20/20C-HS, x2000 voltage amplification), driven by a PC controlled function generator (Tektronix, AFG 2021) fixed at 3 kHz. The amplitude of the sinusoidal waveform was periodically adjusted to maintain the desired plasma power. The high voltage and the resulting current were recorded by a high-

9

voltage probe (Tektronix, P6015A) and a current transformer (Pearson, Model 4100), and recorded by a digital oscilloscope (Picotech, Picoscope 6402D) in order to calculate the power during a number ($n = 4$) of consecutive periods (T):

$$P = \frac{1}{nT} \int_0^{nT} U(t)I(t)\,dt \qquad (1)$$

The gas feed was connected as needed for the particular configuration (see Table 1), and the flow rates were set and controlled by mass flow controllers (Bronkhorst, EL-FLOW Select series) to provide the required flow rates. The reactor effluent was subsequently analysed by a gas chromatograph (Interscience, Compact GC). This GC has two thermal conductivity detector (TCD) channels and one flame ionization detector (FID). The first TCD (TCD B) contains a Rt-Q-Bond column able to separate CO_2 and larger hydrocarbons from the permanent gases, while the second (TCD M) contains a Rt-Q-bond pre-column to delay CO_2 and the larger components, in order to only inject the permanent gases on a Molsieve 5A column and separate them. The FID has a Rtx-1, 5u column to separate and detect (oxygenated) hydrocarbons.
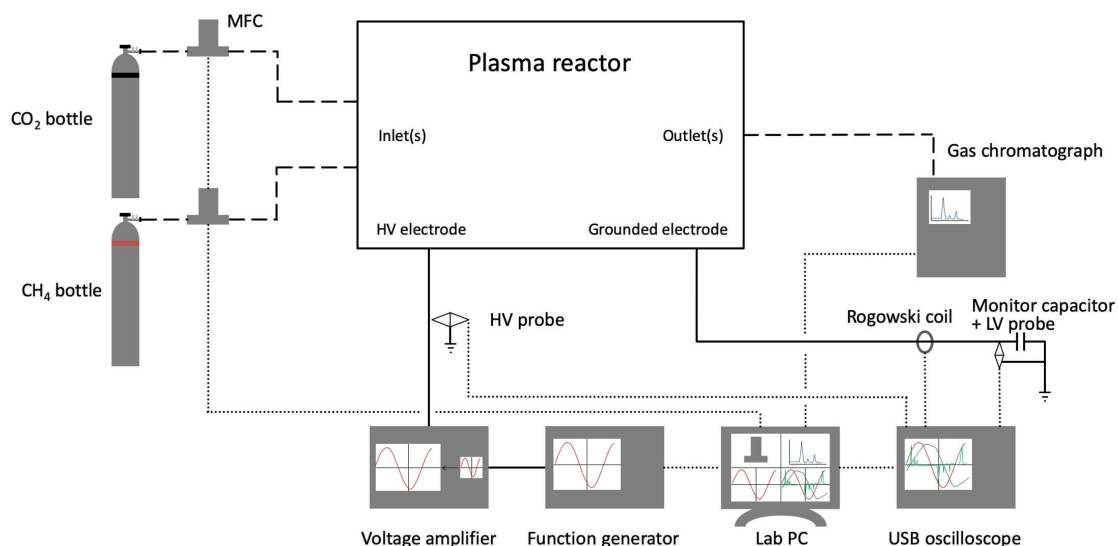
Figure 2: DBD plasma reactor set-up used in this work with analytical equipment.

All measured components are listed in Table 2. Nine peaks could be calibrated by calibration standards (Air Liquide). 22 more peaks could be identified but not calibrated, because either no calibration standard was available (vapor injection) or they coincide with other peaks. Combined peaks for all C2 and C3 hydrocarbons were seen here, as well as three unspecified heptanes. Finally, three peaks remain unknown, and will thus be reported with their peak area to still compare them throughout the measurements.

Table 2: Overview of the components measured by the GC. The components are split into those that are (i) measured, identified, and calibrated, (ii) measured and identified (called "known"), and (iii) only measured but "unkown".

Status	Detector	Components
(i) Calibrated	TCD	CO_2, CO, O_2, CH_4, H_2, Ethane, Ethene, Propane, Ethanol
(ii) Known	TCD	Water, Propene
	FID	C2's, C3's, Isobutane, Methanol, n-Butane, 2-Methylbutaan, 2-Propanol, Acetone, n-Pentane, Diethylether, 2,2-Methylbutane, 1-Propanol, 2-Methylpentane, 3-Methylpentane, n-Hexane, Heptane(1), 1-Butanol, Heptane(2), Cyclohexane, Heptane(3)
(iii) Unknown	FID	1, 2, 3

The CO_2 or CH_4 conversion derived from the GC data was defined as:

$$X_y = \frac{\dot{y}_{in} - \dot{y}_{out}}{\dot{y}_{in}}, \qquad (2)$$

with $\dot{y}$ the molar flow rate of component y, being either CO_2 or CH_4. The total conversion was calculated according to the CO_2 : CH_4 molar ratio of the mixture (A:B):

$$X_{Total} = \frac{A\, X_{CO_2} + B\, X_{CH_4}}{A+B} \qquad (3)$$

Finally, the energy cost (EC), i.e. the amount of energy necessary to convert one mole of reactant mixture, is calculated according to:

$$EC = \frac{SEI.V_m}{X_{Total}}, \qquad (4)$$

11

with SEI the specific energy input, i.e. the ratio of plasma power and volumetric flow rate $\left(SEI = P/\dot{V}\right)$, and V_m the molar volume (22.4 L/mol).

2.4   Experimental method

To ensure (thermal) steady-state behaviour in the reactor, each experiment was operated for 40 min. The temperature of the reactor, measured immediately after shutdown of the voltage, never exceeded 60°C. Each condition was tested in threefold for statistical review, and every time four GC and oscilloscope measurements were recorded as soon as steady-state behaviour was reached. The corresponding error bars were defined as:

$$error = \pm \, S_n \frac{T(p,n_s)}{\sqrt{n_s}}, \qquad (5)$$

with S_n the sample standard deviation of the measurements, n_s the sample size (12), and T the two-tailed inverse of the Student's t-distribution for sample size n_s and probability p set at 95%.

3   Results

The results are split up into two sections to explore the possibilities of adding and mixing CO_2 and CH_4 in the reactor. First we will use the traditional 'one inlet – one outlet' design to set the benchmark for the rest of the paper, and investigate how the dimensions of the reaction zone and the power delivery to the reactor influence the performance. Next we will introduce gradual addition of one of the gas components to the reactor and survey the effect, including studying the impact of pre-activating the individual gases by the plasma and mixing them later in the reactor. All configurations will be tested at standard conditions (see section 2.2) unless stated otherwise.

12

3.1   One inlet – one outlet

3.1.1   L and S configuration

The benchmark for this work is the most simple and traditional configuration, being the one inlet – one outlet reactor in its lengthwise orientation (length > width), denoted as L, as shown in section 2.2. The benchmark conditions are 30 W, 50 mL/min of a 1:1 CO_2 : CH_4 mixture, and 1 bar for reactor dimensions of 100x50x3.5 mm. The results of this benchmark are shown in Figure 3(a). Furthermore, its total conversion will also be plotted as a dotted line where applicable in any further figures, for reference. The CO_2 and CH_4 conversions are 12.9% and 14.6%, respectively, resulting in a total conversion of 13.7%. The main products formed are 6.0% H_2 and 6.4% CO, giving a H_2 : CO ratio of 0.94. This is a bit low to use this gas mixture (syngas) for Fischer-Tropsch synthesis, where a ratio close to 2 is more desirable [31]. Also, 0.094% ethene, 0.97% ethane, 0.16% propane, and 66 ppm ethanol were formed, as can be seen in Figure 3(b), with the exact values listed in Table SI 1 in the supplementary information. In Figure 3(c) we plot the uncalibrated products that were formed and detected on the TCD (propene) and FID. Because the response factor of an FID for non-oxygenated hydrocarbons is proportional to the number of C atoms in the molecule, we can cautiously compare all FID detectable components on a 'mole equivalent basis' by dividing the individual peak areas by their respective carbon number. We can see that the total CH_4-equivalent peak area (i.e. a measuring stick of the total hydrocarbon fractions) is 24.32 x10^4, with the major products being C2 hydrocarbons (83%), followed by C3 hydrocarbons (10%), isobutane (2%), n-butane (2%), and 2-methylbutane (2%); see Table SI 3. All other detectable components have a share lower than 1%. Finally, we calculated the energy cost (EC), i.e. the amount of energy necessary to convert one mole of reactant mixture, and obtained a benchmark value of 1.63 kWh/mol.
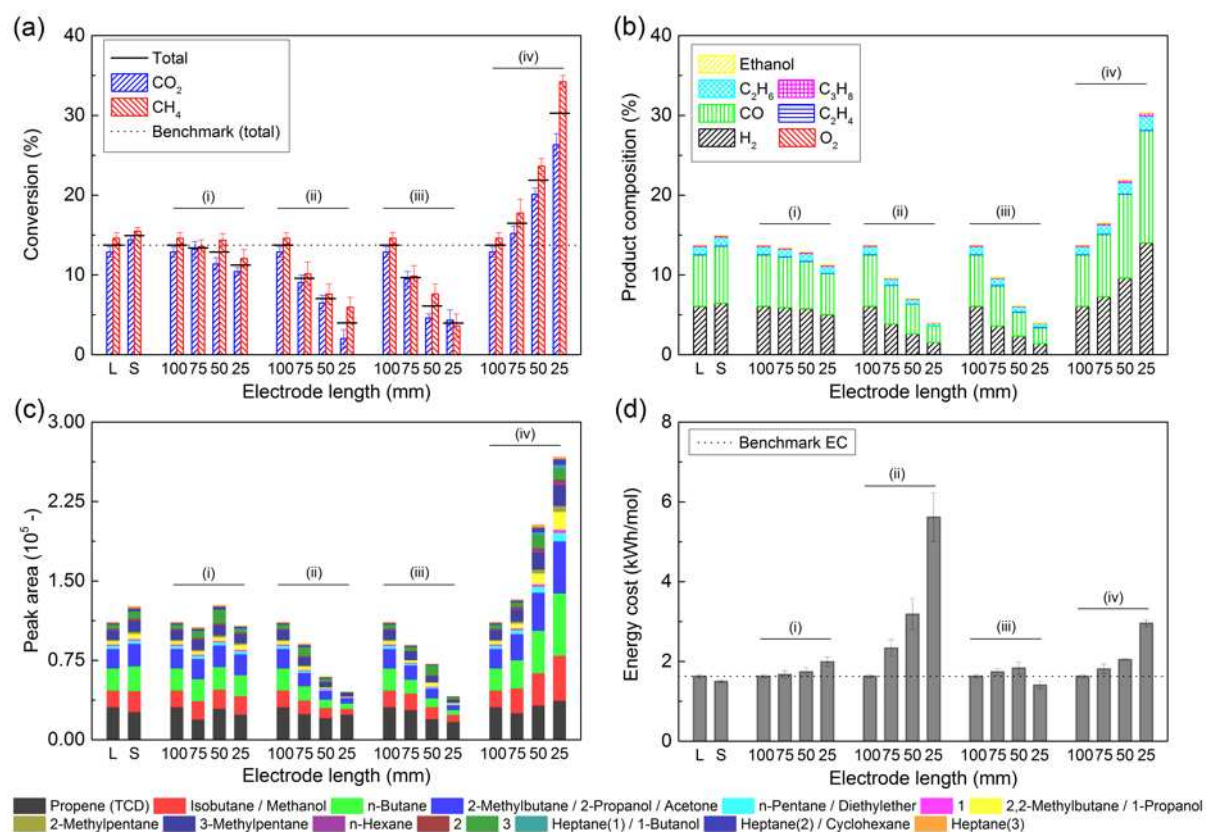
Figure 3: (a) CO₂, CH₄, and total conversion, (b) product composition, (c) peak areas of the uncalibrated gas components, and (d) energy cost of 1:1 DRM, plotted for different reactor geometries, i.e. the benchmark in the long (L) and short (S) configurations, the influence of the electrode length, (i) at constant power (30 W) and flow rate (50 mL/min), (ii) at constant residence time (21 s) and SEI (36 kJ/L), (iii) at constant flow rate (50 mL/min) and power surface density (0.6 W/cm²), and (iv) at constant power (30 W) and residence time (21 s). The total conversion of the 'L configuration' is also indicated with a dotted line, as the benchmark throughout all measurements. All exact values can be found in Table SI 1, Table SI 2, Table SI 3 and Table SI 4 in the supplementary information.

A few modifications can easily be applied to the L configuration within the same operating window. This L configuration is characterized by a relatively long but narrow geometry, giving rise to a small cross-section and thus high gas velocity. A first modification is to shift the general flow of gases by 90 degrees, yielding a relatively short but wide geometry, including a wider gas inlet, so that the gas velocity will be much lower. As a result, the residence time is kept the same. This configuration with the same overall dimensions (50x100x3.5 mm) is denoted as the S configuration and the results are also plotted in Figure 3. Despite having the same operating conditions and thus the same power deposition and residence time, the S

14

configuration shows a slightly improved performance on almost all aspects. The CO_2 and CH_4 conversion increases to 14.4% and 15.5%, respectively, resulting in a total conversion of 14.9%. The H_2 and CO concentrations increase to 6.4% and 7.2%, respectively, but their ratio slightly decreases to 0.90. The hydrocarbon production increases and shifts a bit more towards C3 components. These observations are most likely an effect of the reduced gas velocity, giving more opportunity for diffusion and thus mixing of the products and remaining reactants, as all seven side-inlets are used here to ensure an even flow pattern through this bigger cross-section.

3.1.2   Effect of electrode length

Further modifications within the L configuration are realized by changing the electrode dimensions. Reducing the length of the electrode results not only in a smaller reaction volume, but also the residence time, SEI, and power surface density (PSD; i.e. power per HV electrode area) change. Therefore, we can investigate a few different scenarios by separately changing the plasma power and flow rate or keeping either or both constant. All conditions and associated parameters are listed in Table 3.

Table 3: Conditions used when varying the electrode length. As the electrode becomes shorter, scenario (i) maintains a constant flow rate and power, thus yielding a shorter residence time but constant SEI and larger power surface density (PSD), scenario (ii) proportionally adapts the flow rate and power, to keep the residence time, SEI and PSD constant, scenario (iii) maintains a constant flow rate and uses a proportional power, so keeping the PSD constant, and scenario (iv) uses a proportional flow rate (to keep the residence time constant) and maintains a constant power (yielding a larger SEI and PSD). Note that the electrode length of 100 mm corresponds to the benchmark L configuration.

Scenario	Electrode length (mm)	Reaction volume (cm³)	Flow rate (mL/min)	Residence time (s)	Power (W)	SEI (J/mL)	PSD (W/cm²)
(i)	100 (L)	17.5	50	21	30	36	0.6
	75	13.125	50	15.75	30	36	0.8
	50	8.75	50	10.5	30	36	1.2
	25	4.375	50	5.25	30	36	2.4
(ii)	100 (L)	17.5	50	21	30	36	0.6
	75	13.125	37.5	21	22.5	36	0.6
	50	8.75	25	21	15	36	0.6
	25	4.375	12.5	21	7.5	36	0.6
(iii)	100 (L)	17.5	50	21	30	36	0.6
	75	13.125	50	15.75	22.5	27	0.6
	50	8.75	50	10.5	15	18	0.6
	25	4.375	50	5.25	7.5	9	0.6
(iv)	100 (L)	17.5	50	21	30	36	0.6
	75	13.125	37.5	21	30	48	0.8
	50	8.75	25	21	30	72	1.2
	25	4.375	12.5	21	30	144	2.4

The first scenario (i) investigates the balance of residence time and PSD. Decreasing the electrode length, while keeping the power and flow rate (and the resulting SEI) constant, results in a shorter residence time but also in a higher PSD. This might provide more powerful plasma micro-discharges, because the same amount of energy is applied on a smaller area (or in a smaller volume), and this might compensate for the shorter residence time. The results plotted in Figure 3 show, however, that this is not the case as the total conversion (and thus also total product composition) decreases from 13.7% to 11.2% when the residence time decreases from 21 s to 5.25 s. Still, this is an interesting result, as the drop in conversion is much more limited than the drop in residence time. In our previous work, we investigated the influence of residence time on the conversion of CO_2 and CH_4 in the pure gases, as well as in the mixture (DRM) [32,33] in a coaxial micro DBD reactor, by changing the flow rate while keeping the reaction volume constant. These results showed a more pronounced drop in conversion upon shortening the residence time, compared to the trend seen here. To investigate this in more detail, we performed similar experiments as in [32,33] in the present reactor configuration, with

16

a fixed electrode length of 100 mm and a wide range of flow rates, to vary only the residence time while keeping the PSD constant. The results confirm the trend obtained in our previous work, as can be seen in Figure 4. We see a steady decrease of the conversion for shorter residence times, reaching about 14% at 21 s and only 4% conversion at 5.25 s, which is indeed much more pronounced than in the experiments of scenario (i). Therefore, the higher PSD of scenario (i) in fact results in an enhanced plasma discharge, because the drop was less pronounced than when only varying the residence time, but it cannot entirely compensate for the shorter residence time to provide a better conversion. Since the SEI remains constant in this scenario and the conversion slightly decreases, the EC increases accordingly, up to 2.0 kWh/mol (see Figure 3(d)).
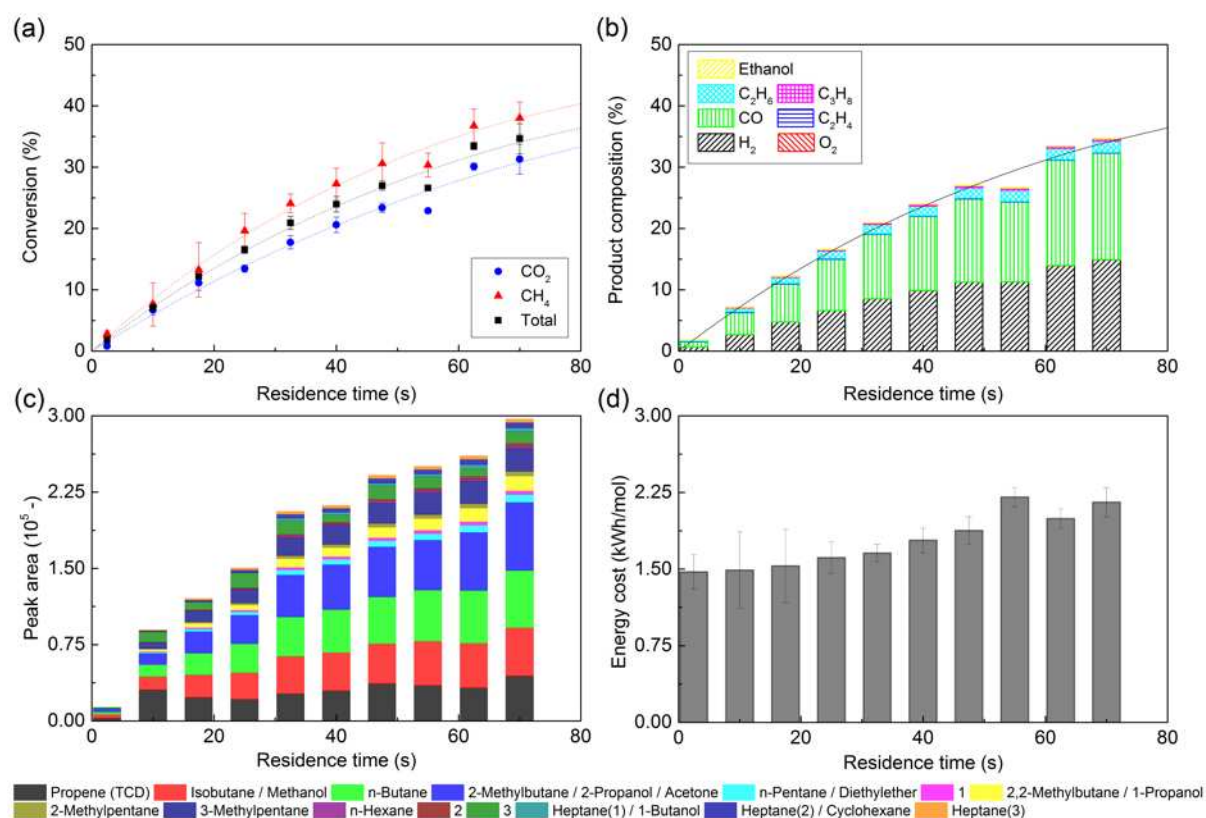
Figure 4: (a) CO_2, CH_4, and total conversion, (b) product composition, (c) peak areas of the uncalibrated gas components, and (d) energy cost for 1:1 DRM, plotted as a function of residence time in the benchmark 'L' reactor at 30 W, by changing the flow rate. All exact values can be found in Table SI 1, Table SI 2, Table SI 3, and Table SI 4 in the supplementary information.

The second scenario (ii) keeps the residence time constant as the electrode gets shorter (i.e. by lowering the flow rate), while also maintaining a constant SEI (i.e. by lowering the power and thus also maintaining a constant PSD). Theoretically, this results in identical cases as the benchmark, with only the gas velocity being different because only the electrode length is reduced but the width is kept constant. The results in Figure 3 show that the drop in power is much more dominant in determining the conversion than the drop in flow rate, at constant SEI and PSD. It has indeed been shown before that the SEI is not always the best "determining parameter" for the energy input [7], although it is commonly used in plasma-based gas conversion [4]. Therefore, the total conversion drops almost linearly from 13.7% to 4%, when the power drops from 30 to 7.5 W, in spite of the constant residence time, SEI, and PSD. Consequently, the product composition decreases for all components (see Figure 3(b,c)), and the EC rises by the same factor, to 5.6 kWh/mol (see Figure 3(d)).

Scenario (iii) maintains a constant flow rate as the electrode becomes shorter, resulting in a shorter residence time, while lowering the power to keep a constant PSD. As a result, the SEI decreases by a factor of four. Both the shorter residence time, as well as the lower power, result in a large decrease in total conversion, from 13.7% to 4%. Surprisingly, these results are comparable to those from scenario (ii) despite using higher flow rates. The EC is slightly lower, because the SEI drops a bit faster than the conversion.

Finally, scenario (iv) evaluates the last combination of maintaining a constant power and adjusting the flow rate to keep the residence time constant. As a result, both the SEI and PSD increase by a factor four. The results in Figure 3 show an increase in total conversion from 13.7% to 30%. Note, however, that this is an increase by only a factor 2.2, while the SEI and PSD increase by a factor 4. This means that almost half of the energy is wasted, resulting in a higher EC of 2.96 kWh/mol. Due to the higher conversion, more products are formed, mainly

18

H_2 and CO (a bit more H_2, thus enhancing the $H_2 : CO$ ratio to 0.99), and shifting the hydrocarbons towards C3.

In summary, concentrating the same amount of power on a smaller electrode, while maintaining the same gas flow rate (scenario i), is not able to improve the conversion, because the higher PSD cannot compensate for the shorter residence time. Also, the power has a more important effect than the flow rate in determining the SEI, but no reduced EC values were found despite enhanced conversions.

3.1.3 Effect of gas mixing ratio

Finally, we investigated the effect of different gas mixing ratios in the one inlet – one outlet reactor. We performed these experiments to compare with the results of the multiple inlets and outlets, where we gradually add the second gas (either CO_2 or CH_4) or have separate injection of CO_2 and CH_4, so that different parts of the reaction zone will exhibit different gas mixing ratios, varying actually between pure CO_2 and pure CH_4. Of course, reactions and diffusion of the produced components will occur at every point in the reactor, so the present measurements render somewhat idealized conditions, but are still interesting to study.

Figure 5 shows the results for different $CO_2 : CH_4$ ratios performed at the standard conditions. Pure CO_2 has a base conversion of 6% and results exclusively in stoichiometric O_2 and CO fractions of 2.10% and 4.20%, respectively. Adding CH_4 to the mixture (6:1 ratio) results in a large increase of the CO_2 conversion to 13%, combined with a large CH_4 conversion of 24.5%, giving an overall conversion of 14%. As a consequence, we see an enhanced CO fraction of 9.06% but only 0.04% O_2 due to further reactions with CH_4-derived products. In addition, we also produce 5.1% H_2, 0.26% ethane, 0.012% propane, and 0.208% ethene. The product share based on the total mole equivalent of the FID peak areas shows the C2 hydrocarbons indeed as the dominant hydrocarbon product (92%), followed by C3 hydrocarbons (2%), isobutane (2%), n-butane (1%), and 2-methylbutane (1%).

19

Gradually adding more CH_4 first enhances the CO_2 conversion up to a maximum of 15% (3:1 ratio), but then it decreases back to 6.3% (1:6 ratio). The CH_4 conversion, on the other hand, steadily decreases towards 7.3% in the pure CH_4 plasma. As a result, the total conversion shows a slight improvement and a maximum at the 3:1 ratio, followed by a steady decrease. The product distribution therefore shifts as more CH_4 is added. The CO fraction gradually decreases from 8.8% (3:1 ratio) to 0% (0:1 ratio), while the O_2 fraction remains near 0% and the H_2 fraction slightly increases to a maximum of 6.1% (1:3 ratio), followed by a decrease to 5.0% (0:1 ratio). The fraction of calibrated hydrocarbons slowly increases towards pure CH_4 where they reach their maximum values of 1.57% ethane, 0.42% propane, and 0.208% ethene. The product distribution of all FID detectable products therefore shifts towards higher carbon numbers with 72% C2, 17% C3, 2% isobutane, 5% n-butane, and 2% 2-methylbutane.

Figure 5: (a) CO_2, CH_4, and total conversion, (b) product composition, (c) peak areas of the uncalibrated gas components, and (d) energy cost, plotted for different CO_2 : CH_4 ratios varying between pure CO_2 and pure CH_4, in the benchmark 'L' reactor at 30 W and 50 mL/min total gas flow rate. All exact values can be found in Table SI 1, Table SI 2, Table SI 3, and Table SI 4 in the supplementary information.

20

These results are consistent with our previous work on the kinetics and equilibria in CO_2 : CH_4 plasmas [32,33], where we found that CO_2 dissociation has a relatively high reaction rate coefficient but a low equilibrium conversion, while CH_4 has a relatively low reaction rate coefficient but a higher equilibrium conversion. This results in similar conversions at the moderate residence time of 21 s, but boosts the total conversion when both of them are combined. More CO_2 effectively promotes the overall reaction rates and thus the conversion, while more CH_4 effectively promotes the equilibrium conversion. This results in a balance of two effects, with apparently CO_2 being slightly dominant in this set-up and conditions, shown by the optimal conversion at a 3:1 (or even 6:1) ratio.

As CH_4 was found to be almost exclusively the hydrocarbon source, optimal hydrocarbon production is therefore only present at higher CH_4 ratios, while conversion-wise, Figure 5 shows that it is indeed more beneficial to operate at CO_2 : CH_4 gas ratios around 6:1 to 3:1. This is also reflected in slightly lower EC-values of 1.5 kWh/mol, as seen in Figure 5(d).

3.2   Multiple inlets and outlets

When multiple elementary reactions occur in a reactor, i.e. reactions in parallel or in series, immediate mixing of the reactants and feeding them in the reactor might not be the most desirable way [19]. Therefore, it can be beneficial to gradually add one of the reactants in order to keep its local concentration low in the reactor, or to introduce both gases at separate locations, so that they can be pre-activated by the plasma before mixing. These effects will be explored below.

3.2.1   Gradual addition of one of the gases

Gradual addition of one of the reactants can be done in our reactor in two ways. The first, denoted by LGA, is gradual addition in the long pathway orientation (similar to configuration L)

21

by using the bottom hole as the main gas inlet, the 14 side holes as the inlets of the gradually added gas, and the top hole as the outlet (see section 2.2). The other way, denoted by SGA, is the equivalent short S configuration by using the left 7 holes as the main gas inlet, the top and bottom holes as the inlet of the second gas, and the right 7 holes as the outlets. Figure 6(a, c, e, and g) shows the result of these configurations where CO_2 is introduced as the main gas and CH_4 as the added gas.

We see that the LGA configuration only slightly improves the total conversion to 14.2% (compared to 13.7% for the benchmark L configuration), which is mainly attributed by the enhanced CH_4 conversion. As a result, primarily the amount of hydrocarbons increases among all products formed. The SGA configuration with its inherent lower gas velocity, however, did improve the performance significantly to 19.2%, resulting in a rise for all products and the lowest EC in this work (1.17 kWh/mol; see figure 6(g)).
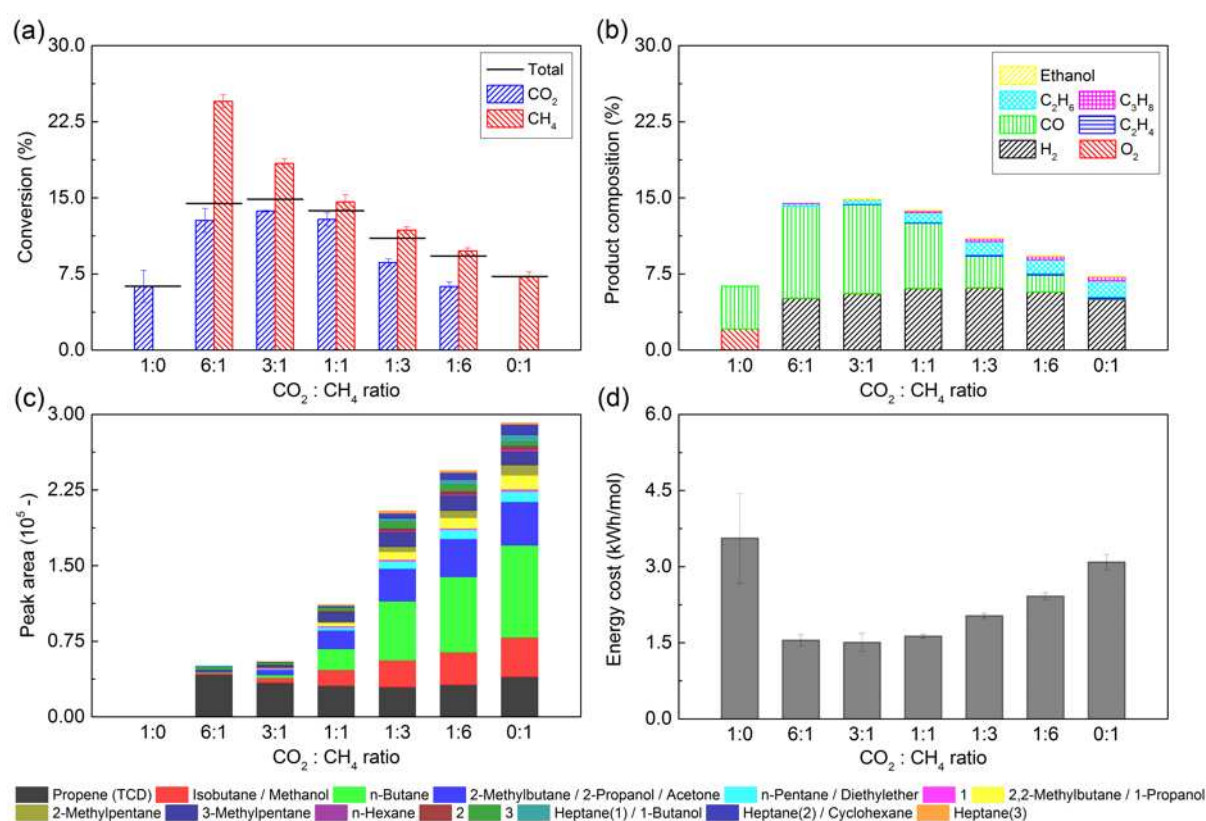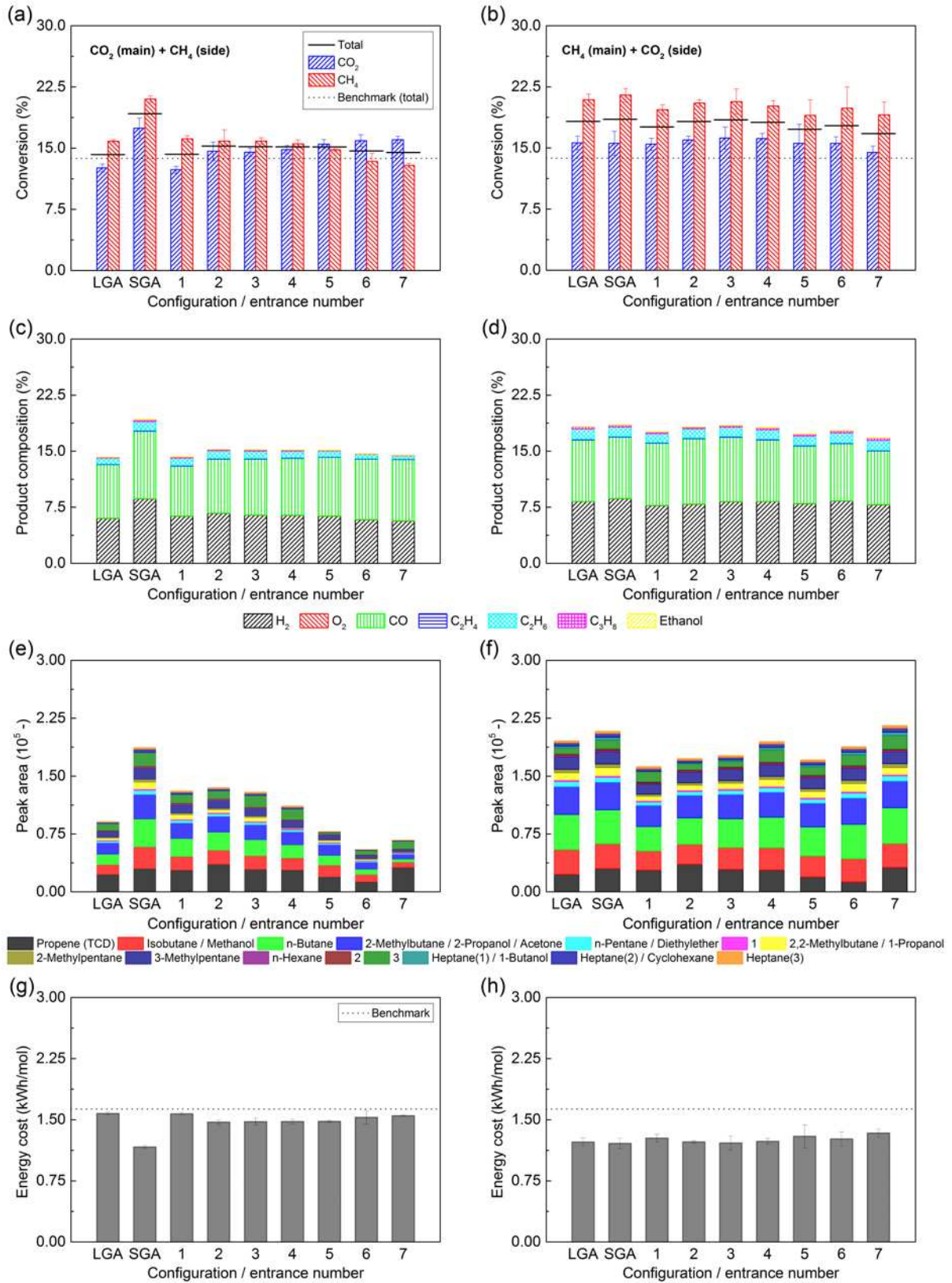
Figure 6: (a and b) CO₂, CH₄, and total conversion, (c and d) product composition, (e and f) peak areas of the uncalibrated gas components, and (g and h) energy cost of 1:1 DRM, plotted for different reactor configurations (see text and Table 1). In (a, c, e, and g) CO₂ is the main gas and CH₄ is the side-added gas, while in (b, d, f, and

23

Introducing CH$_4$ as the main gas and CO$_2$ as the gradually added gas, shows totally different results, see Figure 6(b, d, f, and h). We now also see improved conversion for the LGA configuration (18.3%), and consequently also increased product formation. Compared to the benchmark conversion of 13.7% for the L configuration, and the marginally improved LGA conversion of the reverse gas configuration (14.2%), this is a big leap forward by just mixing the gases differently. Apparently it is preferred to use CH$_4$ as the main gas and keep CO$_2$ at lower local concentrations. Indeed, CH$_4$ will start to become dissociated at the beginning of the reactor at low local CO$_2$: CH$_4$ ratios, by electron impact reactions, and possibly also upon reaction with the CO$_2$ that is gradually being introduced. When CH$_4$ travels further in the reactor, and becomes further converted, while gradually more CO$_2$ will be mixed in, the gas ratio will shift above one and boost the CO$_2$ conversion, in agreement with the results presented in Figure 5. This results in a higher overall conversion. The reverse configuration, i.e. with CO$_2$ as the main gas, starts out at the more optimal gas mixing ratios, but when CO$_2$ is being converted, the ratio drops below one, resulting in a lower total conversion, as depicted in Figure 5. Although both configurations appear similar, our results demonstrate that one is preferred over the other. Comparing both LGA configurations with the SGA configurations suggests that there is a time or velocity dependent factor that is dependant on the gas configuration being used.

Evidently, the gradual addition of one of the components seems useful to improve the total conversion of a DBD plasma reactor. Detailed knowledge on the chemical kinetics, e.g. by numerical modelling [34,35], could help in designing to most optimal configuration.

3.2.2 Introducing both gases at separate locations to allow pre-activation in the plasma

Side addition

In DRM, a direct collision between CO_2 and CH_4 will not result in a reaction between both molecules [34,35]. CO_2 will mainly dissociate in CO and O (although reactions with CH_2 to CH_2O are also possible), while CH_4 will mainly dissociate in CH_3 and H (and other CH_x radicals), and these products will react with each other into oxygenated hydrocarbons [36]. Therefore, it might be beneficial to pre-activate the reactants, to generate reactive or excited species, or intermediate products, before mixing them together. We will first explore this concept by introducing the main gas through the bottom hole, and the second gas through one pair of the seven side inlet pairs. This allows us to vary the amount of pre-activation of both gases.

In Figure 6(a, c, e, and g) we can see the results for CO_2 as the main gas and CH_4 as the added gas at the different inlets. The later CH_4 is added to the reactor, the more CO_2 is converted (12.4% for side inlets 1, vs. 16.0% for side inlets 7) while less CH_4 is converted (16.1% vs. 12.9%). This can be explained by the individual residence times in the reactor, confirmed by computational fluid dynamics (CFD) simulations and similar experimental E-curve measurements for the residence time distribution (RTD) [19], see the supplementary information for the principle and detailed results. Note that we will have (much) higher residence times in the experimental measurements because of delays due to tubing and the trace analyser (an MS in these RTD tests). Consequently, we cannot directly compare the experimental RTD to those simulated, but we can compare at best the relative trends (i.e. time differences between side inlets 1 and 7). The simulated average residence time when using the first side inlets is about 21 s for both gases, while it is about 39 s for CO_2 and 4 s for CH_4 when using the last side inlets (see Table SI7 in the supplementary information). This also yields an average overall residence time of 21 s. Experimentally we also see a decrease in

residence time from 99.1 s (for side inlets 1) to 66.7 s (for side inlets 7) for CH_4. In both cases, i.e. simulations and experiments, the CH_4 residence time is of course much shorter for side inlets 7 compared to side inlets 1, because of the shorter path from inlet to outlet (25 mL/min over short reaction volume), while the CO_2 residence time is longer, because of the lower gas velocity (25 mL/min over almost all reaction volume). It is quite surprising that, even at these very short residence times for CH_4, this gas still reaches a relatively high conversion.

Although both individual conversions shift (up for CO_2 and down for CH_4) when the side inlets are further away from the bottom inlet, the total conversion stays constant within the error bars and is about the same as the LGA configuration. Thus, based on the conversion, the product distribution, and the EC, as seen in Figure 6(a, c and g), we can conclude that it does not really matter which side inlet is used. Only slightly more CO (8.2% vs. 6.7%) and slightly less H_2 (5.7% vs. 6.3%) is produced when CH_4 is introduced later in the reactor (inlets 7 vs. inlets 1). The main effect of changing the inlet position is found in the amount and distribution of hydrocarbons produced, as seen in Figure 6(e). Indeed, the amount of hydrocarbons produced is reduced by a factor two, and the distribution shifts towards lower carbon numbers when CH_4 is introduced later in the reactor.

Changing the gas flow to CH_4 as the main gas and CO_2 as the added gas from the side inlets, gives totally different results, as can be seen in Figure 6(b, d, f, and h). Again, the average residence times vary a lot, being 21 s vs. 38 s for CH_4 (main gas) and 22 s vs. 4 s for CO_2 (added gas), for inlets 1 to 7, respectively, based on our CFD simulations. Experimentally, we see a decrease from 100.2 s to 80.8 s for CO_2. Despite this difference in residence times, the conversions, CO and H_2 formation, and the EC seem to be relatively constant, irrespective of the inlet pair being used, and very similar to those in the LGA and SGA configuration. Again, with the very short residence time of the added gas (i.e. CO_2 here), it is still possible to obtain 15.5% CO_2 conversion. In addition, no significant amounts of O_2 are present in the outlet,

26

indicating that almost all O atoms react within a short time with the CH_4-derived products. Only slight differences are seen in the hydrocarbon production, which increases slightly and the distribution shifts a bit more to C3, upon introducing CO_2 later in the reactor.

These results are rather peculiar. First, the high conversion (of both CO_2 and CH_4) when introducing this gas at side inlets 7, corresponding to a short residence time (3 – 4 s predicted by the CFD simulations), suggests that either the conversion starts early and saturates after some time (but this contradicts the data from Figure 4 and from model calculations [34]), or more mixing is present due to higher diffusion coefficients. Secondly, the total conversion appears constant, irrespective of which side inlet is used, and furthermore, also the individual conversions are constant when CH_4 is the main gas, which is a bit unexpected. It is hard to know exactly how gas fractions shift along the reactor due to individual conversion, mixing, and reacting further on. Perhaps the local $CO_2 : CH_4$ ratios are accidently in the perfect range for high reaction rates, resulting in unusually high conversion at short residence time. Further investigations with spectroscopic techniques are needed to uncover this phenomenon.

Separate pre-activation zones

We further investigate the concept of gas pre-activation with the extreme case of opposite inlets, yielding purely individual plasma activation zones for CO_2 and CH_4, that only mix right at the end. In practice, we use the bottom hole of the reactor as the inlet for the first gas, the top hole as the inlet of the second gas, and the centre side holes (see Table 1) as the outlets. By changing the width of the outlets, we influence the size of the mixing zone. This yields a long reactor either with narrow or wide outlets, denoted as LSN and LSW, respectively (see Table 1). In addition, we shift the inlets and outlets by 90°, resulting in a short reactor with narrow and wide outlets, denoted as SSN and SSW, respectively.

27
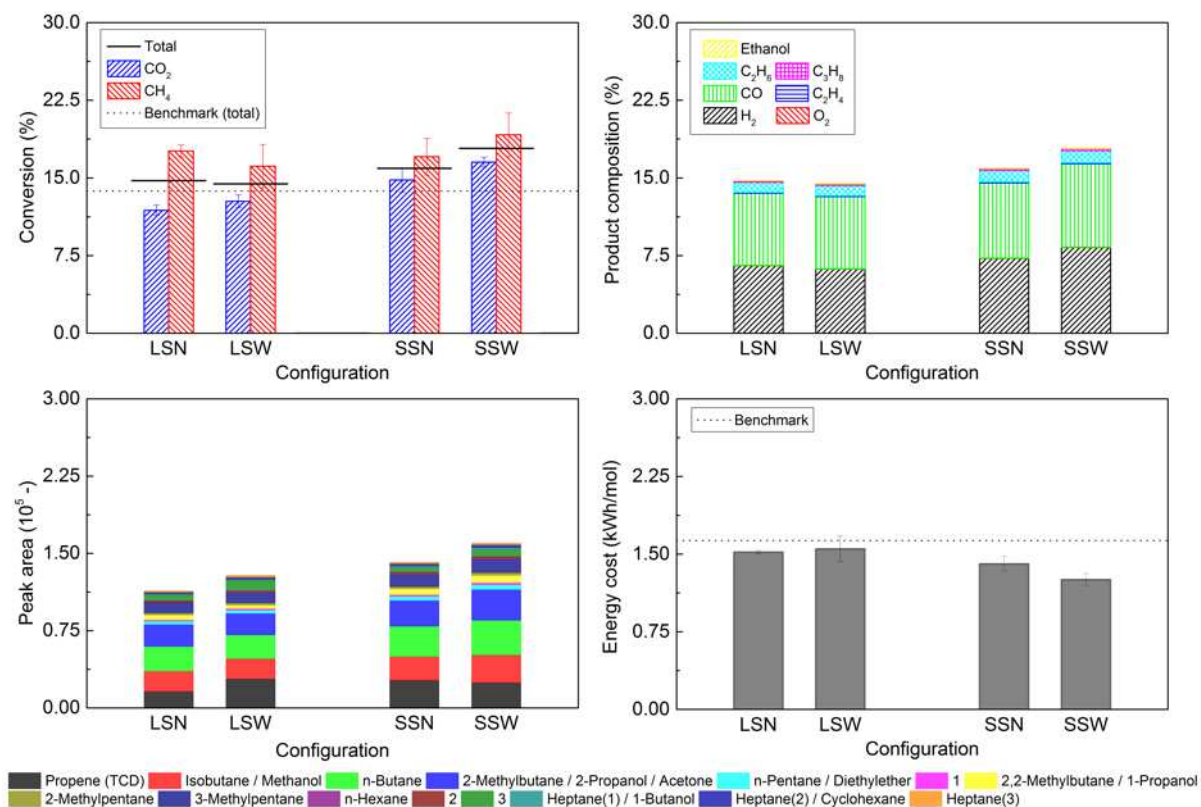
Figure 7: (a) CO$_2$, CH$_4$, and total conversion, (b) product composition, (c) peak areas of the uncalibrated gas components, and (d) energy cost of 1:1 DRM, plotted for different reactor configurations, where CO$_2$ and CH$_4$ are inserted through opposite inlets and are separately activated in the plasma before mixing. For the exact configuration, see Table 1. All experiments are performed at 30 W and 50 mL/min total flow rate. All exact values can be found in Table SI 1, Table SI 2, Table SI 3, and Table SI 4 in the supplementary information.

Figure 7 shows that the LSN configuration performs a bit better than the benchmark L configuration, i.e. the total conversion reaches 14.7% compared to 13.7% in the benchmark. This is due to a higher CH$_4$ conversion, while the CO$_2$ conversion stays the same. Enlarging the mixing zone in the LSW configuration slightly enhances the CO$_2$ conversion but reduces the CH$_4$ conversion, resulting in a small drop of the total conversion to 14%.

Using the 'short' orientation of the reactor again results in slightly better results. The SSN configuration reaches a total conversion of 16%, while the SSW configuration performs even better, with 18% total conversion. This is probably again due to the lower gas velocity, but in addition, the S orientation allows for a larger mixing zone, resulting in more conversion upon

mixing, at the more optimal 'around 1:1' ratios. It is interesting to note that even these short mixing zones allow sufficient reaction between the CO_2 and CH_4 decomposition products, as is evident by the lack of O_2 in the outlet.

Finally, we see somewhat higher product formation, and the product ratios slightly shift towards higher carbon numbers, while the energy cost drops to 1.26 kWh/mol.

4   Discussion

The results in section 3 have shown that definite improvements on both conversion and product composition are possible by changing the reactor geometry. The most likely optimal configuration would be an SGA reactor with optimised (more) side-inlets, preferably with CH_4 as the main gas and CO_2 as the co-reactant. Extra tests with slightly altered CO_2:CH_4 mixing ratio towards 3:1 could improve the conversion even more.

A lot of research has been performed on improving the performance of DBD reactors through different strategies, but to our knowledge with no major steps forward of bringing DBD plasma technology closer to industrial use (e.g. [7,8,17,18,9–16]). The hypothesis of our work was that more drastic improvements to the reactor design could offer a leap forward to further advance from. We have shown how reactor geometry and gradual addition of the reactant gases can significantly alter the performance of a DBD plasma reactor and the product composition, while still using the same feed, but the actual conversion and energy cost improvements are still limited compared to the reference reactor. Therefore, we have to conclude that despite the interesting findings of our work, even bigger improvements are required to make DBD plasma-based DRM a competing technology.

The question arises whether knowledge from this work can be transferred to other gas mixtures. Our findings from section 3.1 can indeed be transferred, because in these configurations fundamental "plasma properties", i.e. reaction time and plasma density, are

29

varied. Our findings from section 3.2, on the other hand, apply to individual reactions and mixing behaviours of the individual gasses, and therefore, these results cannot simply be transferred to other chemical conversions. For instance, we evaluated the same configuration of section 3.2 to an N_2/H_2 plasma for NH_3 synthesis, and found no positive effects of varying the configurations. This can be explained because pure N_2 and H_2, occurring in their separate reaction zones before mixing, do not generate long-living products, but only short-living atoms, ions and excited species. Therefore, when they are not being mixed, this corresponds to a waste of power and reaction time, resulting in decreased conversions. Thus, non-reactive molecules will not benefit from any time not being mixed. However, in the case of reactive molecules, the general idea that alternative gas mixing can optimise performance is still valid, but the actual changes will depend on the specific chemistry.

The exact origin of the changes in reactor performance observed in this work is still not entirely understood. How do these different configurations influence the reaction kinetics and equilibrium position? Recently we developed a method of retrieving more fundamental kinetics data on plasma reactor performance, by recording the conversion over an extended residence time range [32,33]. Fitting these data by a generalised fit equation reveals the overall rate coefficient, its individual loss and formation components, and the position of the so-called 'partial chemical equilibrium'. We applied this method in Figure 4, for the L-configuration, to test whether changing the residence time by means of the flow rate is equal to changing it by means of the reactor length. Following the procedure of our previous DRM kinetics work [33], this L-configuration yields an overall reaction rate coefficient of 0.015 s^{-1} $\pm$ 0.004 s^{-1}, with equilibrium conversion around 53%. These values are lower than for the coaxial micro-DBD reactor studied in [33] (0.088 s^{-1} $\pm$ 0.003 s^{-1} and 75.4% $\pm$ 0.6% for 1:1 CO_2:CH_4 ratio), due to the bigger gap size. This method is very time-consuming, because it requires studying at multiple and long residence times, so it is beyond the scope of this paper, but in the future we might be able to apply such a study to the various reactor configurations in this paper, with the

30

aim to reveal the more precise nature of the altered reactor performance, i.e. changes in rate coefficients and/or position of the equilibrium.

When looking for the industrial application of alternative reactor configurations, and perhaps also other types of plasma reactors, we have to consider several different aspects. Chemically speaking, the configuration yielding the highest conversion at the lowest energy cost is the most optimal configuration for scaling-up to higher throughputs. However, from an engineering point of view, we need to focus our attention to the performance vs. complexity balance, when looking at scale-up possibilities. Indeed, the added complexity of the novel design must be small enough, so that it does not counteract the performance enhancement. At this moment, the most suitable method for allowing more throughput in DBD reactors is scaling the length and width (or tube circumference for co-axial design) of the reactor, and/or putting multiple units in parallel. It is important to realize that the gap dimension has to stay within the micrometre to millimetre range, to limit the required discharge voltage. Taking this aspect into account, it seems that the extra complexity of adding multiple side inlets to an already semi-complex parallel multi-DBD device, such as the industrial ozone generators [6], may not outweigh the performance benefits. An economical and engineering analysis should be made to evaluate whether the standard 'one inlet – one outlet' configuration would still remain the best option or whether multiple side inlets would be feasible for up-scaling.

In general, it may well be that other plasma reactor types, besides DBD, are more promising for DRM, more specifically gliding arc plasmas [37–39], as well as microwave plasmas [40–46], nanosecond pulsed plasmas [47], and atmospheric pressure glow discharges [48] (based on the good results obtained for CO_2 splitting). Indeed, these so-called warm plasmas exhibit much higher energy efficiency (see detailed assessment in [4]). The reason is that they are characterized by higher populations of the vibrationally excited levels, which provide the most efficient dissociation pathway, and they operate at higher temperatures, so that the thermal

31

dissociation reactions are also faster. On the other hand, the higher temperature also reduces the overpopulation of the vibrational levels. Moreover, it is less straightforward to integrate catalysts in these warm plasmas, due to their higher temperatures; hence, for plasma catalysis, DBD plasmas are much better suited.

We believe that overall the optimal plasma reactor should combine a high conversion with high energy efficiency, and be compatible with catalysts, to provide high product selectivity. The conversion should be enhanced by increasing the fraction of gas treated by the plasma, i.e., by smart plasma reactor design (including gas inlet/outlet), based on fluid dynamics simulations, as demonstrated partly in this paper, as well as in e.g. [48,49].

As far as the energy efficiency is concerned, in theory, the highest values can be reached when the reduced electric field (i.e., electric field divided by gas number density, typically expressed in Townsend, with 1 Td = 10^{-21} Vm²) in the plasma is around 50 Td or below, combined with a high plasma power (to maximize vibrational excitation) and with a low gas temperature (to minimize vibrational losses upon collision with other gas molecules), or in other words, a strong vibrational-translational (VT) non-equilibrium [50]. However, both experiments and modelling have revealed that in warm plasmas at (sub)atmospheric pressure the conversion proceeds mainly by thermal reactions, and the vibrational distribution is in equilibrium with the gas temperature (VT-equilibrium) [40–45,50–52]. DBD plasmas operate at much lower temperature, so they could in theory give rise to more pronounced VT non-equilibrium, if they can operate at a reduced electric field that promotes vibrational excitation. However, DBD reactors typically operate at reduced electric fields above 200 Td, where the electron energy is rather used for other processes than vibrational excitation of the molecules. Hence, major research efforts should be devoted, e.g. by designing new power supplies, to tune DBD conditions into producing the right reduced electric field (and thus electron energy) for maximizing vibrational excitation. This is, however, beyond the scope of our present paper.

Finally, in terms of product selectivity, when targeting higher hydrocarbons or oxygenates, the plasma will need to be combined with catalysts, because otherwise the DRM reaction will mainly produce syngas. For this purpose, plasma reactors must be designed to enable optimised transport of plasma species to the catalyst surface, and DBD plasmas are in general most suited for this. However, in addition, catalysts must be developed which are suited for surface reactions of reactive plasma species (i.e. radicals, electronically and vibrationally excited molecules, electrons, ions). These catalysts are most likely different from thermal catalysts. Therefore, more insight in the plasma-catalyst interactions is crucial for designing catalysts tailored to the plasma environment [53,54].

In conclusion, plasma-based DRM is quite promising, but the complex mechanisms require more fundamental investigations towards the optimum plasma reactor configuration. We believe that modelling-based plasma reactor design is key to realize these goals.

5   Conclusion

In this paper we present a novel multi-inlet/outlet parallel plate DBD plasma reactor that we have designed to achieve different gas flow and mixing patterns, and to quickly change the geometry of the reaction volume. This allows us to investigate how the shape and length of the reaction zone, gradual gas addition, and the method of mixing CO_2 and CH_4 can influence the conversion, energy cost, and product composition of dry reforming of methane (DRM).

First we presented the results of a benchmark reactor (long pathway L configuration, with one inlet and outlet for both gases combined), yielding a total conversion of 13.7%. Using the same reactor dimensions but in the short orientation (S configuration) can slightly improve the conversion up to 14.9%, which is attributed to the lower gas velocities (allowing more reaction of the plasma components) as a result of the wider cross section, because all other parameters, including the residence time, are kept constant.

33

Subsequently we modified the length of the reaction zone by changing the electrode length, and we varied the operating parameters (total gas flow rate and power), resulting in various parameters being kept constant or varied, i.e. residence time, specific energy input (SEI), and power surface density (PSD). Concentrating the same amount of power on a smaller electrode (hence higher PSD), while maintaining the same flow rate (constant SEI, but shorter residence time), cannot improve the conversion, because the higher PSD cannot compensate for the shorter residence time. Further permutations of flow rate and power, by either proportionally varying them or keeping them constant, thereby affecting the residence time, SEI, and PSD, showed that the power has a more important effect than the flow rate in determining the SEI. The same power and residence time, but shorter electrode length and thus higher PSD, significantly enhanced the conversion (up to 30% for an electrode length four times smaller than the standard length, i.e. 25 vs. 100 mm), but at the expense of a higher energy cost (i.e. 2.96 kWh/mol at 25 mm electrode length, and 1.63 kWh/mol at 100 mm electrode length).

Varying the CO_2 : CH_4 ratio in the standard (benchmark) geometry revealed that the optimum ratio is between 6:1 and 3:1, and up to 1:1, due to more optimal kinetics at these ratios. This information was very valuable to investigate the effect of both separate and gradual addition of one of the gases. Indeed, the latter shifts the local gas mixing ratios while still maintaining an overall 1:1 ratio as input in the reactor.

Our results show that gradual addition of one of the gases, i.e. via 14 side inlets along the length of the reactor, improves the conversion, but the extent of the improvement highly depends on which gas is used as main gas and added gas (generally higher with CH_4 as main gas), as well as on the long (LGA) or short (SGA) orientation of the reactor (effect by CO_2 as main gas). Pre-activation of the main gas, by delaying a separate side addition of the other gas via one pair of side inlets, showed improvements when CH_4 was used as the main gas, although we did not see a significant influence of the position of the inlet. Total conversions up

34

to 19.2% were obtained in this way at the same standard conditions as the benchmark (yielding only 13.7%), while the EC was improved in the same way, from 1.63 kWh/mol for the benchmark, down to 1.17 kWh/mol for these modifications of gradual or separate gas addition through only one set of inlets.

Finally, pre-activation of the separate gases by using inlets from opposite sides in the reactor, with last-minute mixing of the products, was evaluated as an extreme case of separate addition. Improved conversions up to 18% were found, depending on the orientation and size of the mixing zone. No negative effects were noticed, despite the short time of reactant mixing.

These results show that improvements in the DBD reactor performance for DRM can be made by simple variations in the geometry of the DBD reactor, especially by varying the way of combining the reactants. Nevertheless, the improvements shown for this DBD reactor configuration remain limited, and larger improvements are required to make DBD plasma-based DRM a competing technology.

Acknowledgements

References

[1]   J. Van Durme, J. Dewulf, C. Leys, H. Van Langenhove, Combining non-thermal plasma with heterogeneous catalysis in waste gas treatment: A review, Appl. Catal. B Environ. 78 (2008) 324–333. doi:10.1016/j.apcatb.2007.09.035.

[2]   H.-H. Kim, Nonthermal plasma processing for air-pollution control: A historical review, current issues, and future prospects, Plasma Process. Polym. 1 (2004) 91–110.

35

doi:10.1002/ppap.200400028.

[3] B.S.S. Patil, Q. Wang, V. Hessel, J. Lang, Plasma N2-fixation: 1900–2014, Catal. Today. 256 (2015) 49–66. doi:10.1016/j.cattod.2015.05.005.

[4] R. Snoeckx, A. Bogaerts, Plasma technology – a novel solution for CO2 conversion?, Chem. Soc. Rev. 46 (2017) 5805–5863. doi:10.1039/C6CS00066E.

[5] A. Bogaerts, E.C. Neyts, Plasma Technology: An Emerging Technology for Energy Storage, ACS Energy Lett. 3 (2018) 1013–1027. doi:10.1021/acsenergylett.8b00184.

[6] U. Kogelschatz, Dielectric-barrier discharges: Their history, discharge physics, and industrial applications, Plasma Chem. Plasma Process. 23 (2003) 1–46. doi:10.1023/A:1022470901385.

[7] R. Aerts, W. Somers, A. Bogaerts, Carbon Dioxide Splitting in a Dielectric Barrier Discharge Plasma: A Combined Experimental and Computational Study, ChemSusChem. 8 (2015) 702–716. doi:10.1002/cssc.201402818.

[8] Y. Uytdenhouwen, S. Van Alphen, I. Michielsen, V. Meynen, P. Cool, A. Bogaerts, A packed-bed DBD micro plasma reactor for CO2 dissociation: Does size matter?, Chem. Eng. J. 348 (2018) 557–568. doi:10.1016/j.cej.2018.04.210.

[9] A. Ozkan, T. Dufour, G. Arnoult, P. De Keyzer, A. Bogaerts, F. Reniers, CO2-CH4 conversion and syngas formation at atmospheric pressure using a multi-electrode dielectric barrier discharge, J. CO2 Util. 9 (2015) 74–81. doi:10.1016/j.jcou.2015.01.002.

[10] A. Ozkan, T. Dufour, T. Silva, N. Britun, R. Snyders, F. Reniers, A. Bogaerts, DBD in burst mode: Solution for more efficient CO2 conversion?, Plasma Sources Sci. Technol. 25 (2016). doi:10.1088/0963-0252/25/5/055005.

36

[11]   X. Tu, J.C.C. Whitehead, Plasma-catalytic dry reforming of methane in an atmospheric dielectric barrier discharge: Understanding the synergistic effect at low temperature, Appl. Catal. B Environ. 125 (2012) 439–448. doi:10.1016/j.apcatb.2012.06.006.

[12]   T. Butterworth, R. Elder, R. Allen, Effects of particle size on CO_2 reduction and discharge characteristics in a packed bed plasma reactor, Chem. Eng. J. 293 (2016) 55–67. doi:10.1016/j.cej.2016.02.047.

[13]   I. Michielsen, Y. Uytdenhouwen, J. Pype, B. Michielsen, J. Mertens, F. Reniers, V. Meynen, A. Bogaerts, CO_2 dissociation in a packed bed DBD reactor: First steps towards a better understanding of plasma catalysis, Chem. Eng. J. 326 (2017) 477–488. doi:10.1016/j.cej.2017.05.177.

[14]   X. Duan, Z. Hu, Y. Li, B. Wang, Effect of dielectric packing materials on the decomposition of carbon dioxide using DBD microplasma reactor, AIChE J. 61 (2015) 898–903. doi:10.1002/aic.

[15]   D. Mei, X. Zhu, Y. He, J.D. Yan, X. Tu, Plasma-assisted conversion of CO_2 in a dielectric barrier discharge reactor : understanding the effect of packing materials, Plasma Sources Sci. Technol. 24 (2015) 15011. doi:10.1088/0963-0252/24/1/015011.

[16]   I. Michielsen, Y. Uytdenhouwen, A. Bogaerts, V. Meynen, Altering Conversion and Product Selectivity of Dry Reforming of Methane in a Dielectric Barrier Discharge by Changing the Dielectric Packing Material, Catalysts. 9 (2019) 51. doi:10.3390/catal9010051.

[17]   M.D. Bai, X.Y. Bai, Z.T. Zhang, B. Mingdong, B. Xiyao, Z. Zhitao, Synthesis of ammonia in a strong electric field discharge at ambient pressure, Plasma Chem. Plasma Process. 20 (2000) 511–520.

[18] A. Ozkan, A. Bogaerts, F. Reniers, Routes to increase the conversion and the energy efficiency in the splitting of CO2 by a dielectric barrier discharge, J. Phys. D. Appl. Phys. 50 (2017) 084004. doi:10.1088/1361-6463/aa562c.

[19] O. Levenspiel, Chemical Reaction Engineering Third Edition, 1999. doi:10.1021/ie990488g.

[20] T. Mizushima, K. Matsumoto, J.I. Sugoh, H. Ohkita, N. Kakuta, Tubular membrane-like catalyst for reactor with dielectric-barrier- discharge plasma and its performance in ammonia synthesis, Appl. Catal. A Gen. 265 (2004) 53–59. doi:10.1016/j.apcata.2004.01.002.

[21] H.H. Kim, Y. Teramoto, A. Ogata, H. Takagi, T. Nanba, Atmospheric-pressure nonthermal plasma synthesis of ammonia over ruthenium catalysts, Plasma Process. Polym. 14 (2017) 1–9. doi:10.1002/ppap.201600157.

[22] M. Bai, Z. Zhang, X. Bai, M. Bai, W. Ning, Plasma Synthesis of Ammonia With a Microgap Dielectric Barrier Discharge at Ambient Pressure, IEEE Trans. Plasma Sci. 31 (2003) 1285–1291. doi:10.1109/TPS.2003.818761.

[23] P. Peng, Y. Li, Y. Cheng, S. Deng, P. Chen, R. Ruan, Atmospheric Pressure Ammonia Synthesis Using Non-thermal Plasma Assisted Catalysis, Plasma Chem. Plasma Process. 36 (2016) 1201–1210. doi:10.1007/s11090-016-9713-6.

[24] Q. Wang, Y. Cheng, Y. Jin, Dry reforming of methane in an atmospheric pressure plasma fluidized bed with Ni/γ-Al2O3 catalyst, Catal. Today. 148 (2009) 275–282. doi:10.1016/j.cattod.2009.08.008.

[25] T. Mizushima, K. Matsumoto, H. Ohkita, N. Kakuta, Catalytic effects of metal-loaded membrane-like alumina tubes on ammonia synthesis in atmospheric pressure plasma

by dielectric barrier discharge, Plasma Chem. Plasma Process. 27 (2007) 1–11. doi:10.1007/s11090-006-9034-2.

[26] C. Subrahmanyam, M. Magureanu, a. Renken, L. Kiwi-Minsker, Catalytic abatement of volatile organic compounds assisted by non-thermal plasma. Part 1. A novel dielectric barrier discharge reactor containing catalytic electrode, Appl. Catal. B Environ. 65 (2006) 150–156. doi:10.1016/j.apcatb.2006.01.006.

[27] S. Sato, K. Hensel, H. Hayashi, K. Takashima, A. Mizuno, Honeycomb discharge for diesel exhaust cleaning, J. Electrostat. 67 (2009) 77–83. doi:10.1016/j.elstat.2009.02.004.

[28] S. Mori, N. Matsuura, L.L. Tun, M. Suzuki, Direct Synthesis of Carbon Nanotubes from Only CO2 by a Hybrid Reactor of Dielectric Barrier Discharge and Solid Oxide Electrolyser Cell, Plasma Chem. Plasma Process. 36 (2016) 231–239. doi:10.1007/s11090-015-9681-2.

[29] A. Huang, G. Xia, J. Wang, S.L. Suib, Y. Hayashi, H. Matsumoto, CO2 reforming of CH4 by atmospheric pressure AC discharge plasmas, J. Catal. 189 (2000) 349–359. doi:10.1006/jcat.1999.2684.

[30] G.G. Xia, J.Y. Wang, A. Huang, S.L. Suib, Y. Hayashi, H. Matsumoto, A novel Y-type reactor for selective excitation of atmospheric pressure glow discharge plasma, Rev. Sci. Instrum. 72 (2001) 1383–1390. doi:10.1063/1.1340557.

[31] T. Kaneko, F. Derbyshire, E. Makino, D. Gray, M. Tamura, K. Li, Coal Liquefaction, in: Ullmann's Encycl. Ind. Chem., Wiley-VCH Verlag GmbH & Co. KGaA, Weinheim, Germany, 2012: p. 96. doi:10.1002/14356007.a07_197.pub2.

[32] Y. Uytdenhouwen, K.M. Bal, I. Michielsen, E.C. Neyts, V. Meynen, P. Cool, A. Bogaerts,

How process parameters and packing materials tune chemical equilibrium and kinetics in plasma-based CO2 conversion, Chem. Eng. J. 372 (2019) 1253–1264. doi:10.1016/j.cej.2019.05.008.

[33] Y. Uytdenhouwen, K.M. Bal, E.C. Neyts, V. Meynen, P. Cool, A. Bogaerts, On the kinetics and equilibria of plasma-based dry reforming of methane., Chem. Eng. J. Under revi (2020) 1–38.

[34] C. De Bie, J. Van Dijk, A. Bogaerts, The Dominant Pathways for the Conversion of Methane into Oxygenates and Syngas in an Atmospheric Pressure Dielectric Barrier Discharge, J. Phys. Chem. C. 119 (2015) 22331–22350. doi:10.1021/acs.jpcc.5b06515.

[35] R. Snoeckx, R. Aerts, X. Tu, A. Bogaerts, Plasma-Based Dry Reforming: A Computational Study Ranging from the Nanoseconds to Seconds Time Scale, J. Phys. Chem. C. 117 (2013) 4957–4970. doi:10.1021/jp311912b.

[36] A. Bogaerts, C. De Bie, R. Snoeckx, T. Kozák, Plasma based CO2 and CH4 conversion: A modeling perspective, Plasma Process. Polym. 14 (2017). doi:10.1002/ppap.201600070.

[37] K. Li, J.-L. Liu, X.-S. Li, X. Zhu, A.-M. Zhu, Warm plasma catalytic reforming of biogas in a heat-insulated reactor: Dramatic energy efficiency and catalyst auto-reduction, Chem. Eng. J. 288 (2016) 671–679. doi:10.1016/j.cej.2015.12.036.

[38] E. Cleiren, S. Heijkers, M. Ramakers, A. Bogaerts, Dry Reforming of Methane in a Gliding Arc Plasmatron: Towards a Better Understanding of the Plasma Chemistry, ChemSusChem. (2017). doi:10.1002/cssc.201701274.

[39] J. Slaets, M. Aghaei, S. Ceulemans, S. Van Alphen, A. Bogaerts, CO2 and CH4 conversion in "real" gas mixtures in a gliding arc plasmatron: how do N2 and O2 affect

the performance?, Green Chem. 22 (2020) 1366–1377. doi:10.1039/C9GC03743H.

[40] G.J. van Rooij, D.C.M. van den Bekerom, N. den Harder, T. Minea, G. Berden, W.A. Bongers, R. Engeln, M.F. Graswinckel, E. Zoethout, M.C.M. van de Sanden, Taming microwave plasma to beat thermodynamics in CO2 dissociation, Faraday Discuss. 183 (2015) 233–248. doi:10.1039/C5FD00045A.

[41] W. Bongers, H. Bouwmeester, B. Wolf, F. Peeters, S. Welzel, D. van den Bekerom, N. den Harder, A. Goede, M. Graswinckel, P.W. Groen, J. Kopecki, M. Leins, G. van Rooij, A. Schulz, M. Walker, R. van de Sanden, Plasma-driven dissociation of CO2 for fuel synthesis, Plasma Process. Polym. 14 (2017) 1600126. doi:10.1002/ppap.201600126.

[42] N. den Harder, D.C.M. van den Bekerom, R.S. Al, M.F. Graswinckel, J.M. Palomares, F.J.J. Peeters, S. Ponduri, T. Minea, W.A. Bongers, M.C.M. van de Sanden, G.J. van Rooij, Homogeneous CO2 conversion by microwave plasma: Wave propagation and diagnostics, Plasma Process. Polym. 14 (2017) 1–24. doi:10.1002/ppap.201600120.

[43] D.C.M. van den Bekerom, J.M.P. Linares, T. Verreycken, E.M. van Veldhuizen, S. Nijdam, G. Berden, W.A. Bongers, M.C.M. van de Sanden, G.J. van Rooij, The importance of thermal dissociation in CO2 microwave discharges investigated by power pulsing and rotational Raman scattering, Plasma Sources Sci. Technol. 28 (2019) 055015. doi:10.1088/1361-6595/aaf519.

[44] A.J. Wolf, T.W.H. Righart, F.J.J. Peeters, P.W.C. Groen, M.C.M. van de Sanden, W.A. Bongers, Characterization of CO2 microwave plasma based on the phenomenon of skin-depth-limited contraction, Plasma Sources Sci. Technol. 28 (2019) 115022. doi:10.1088/1361-6595/ab4e61.

[45] A.J. Wolf, T.W.H. Righart, F.J.J. Peeters, W.A. Bongers, M.C.M. van de Sanden, Implications of thermo-chemical instability on the contracted modes in CO2 microwave

41

plasmas, Plasma Sources Sci. Technol. 29 (2020) 025005. doi:10.1088/1361-6595/ab5eca.

[46] D.C.M. van den Bekerom, A. van de Steeg, M.C.M. van de Sanden, G.J. van Rooij, Mode resolved heating dynamics in pulsed microwave CO_2 plasma from laser Raman scattering, J. Phys. D. Appl. Phys. 53 (2020) 054002. doi:10.1088/1361-6463/ab5311.

[47] C. Montesano, S. Quercetti, L.M. Martini, G. Dilecce, P. Tosi, The effect of different pulse patterns on the plasma reduction of CO_2 for a nanosecond discharge, J. CO_2 Util. 39 (2020) 101157. doi:10.1016/j.jcou.2020.101157.

[48] G. Trenchev, A. Nikiforov, W. Wang, S. Kolev, A. Bogaerts, Atmospheric pressure glow discharge for CO_2 conversion: Model-based exploration of the optimum reactor configuration, Chem. Eng. J. 362 (2019) 830–841. doi:10.1016/j.cej.2019.01.091.

[49] G. Trenchev, A. Bogaerts, Dual-vortex plasmatron: A novel plasma source for CO_2 conversion, J. CO_2 Util. 39 (2020) 101152. doi:10.1016/j.jcou.2020.03.002.

[50] A. Berthelot, A. Bogaerts, Modeling of CO_2 Splitting in a Microwave Plasma: How to Improve the Conversion and Energy Efficiency, J. Phys. Chem. C. 121 (2017) 8236–8251. doi:10.1021/acs.jpcc.6b12840.

[51] S. Heijkers, A. Bogaerts, CO_2 Conversion in a Gliding Arc Plasmatron: Elucidating the Chemistry through Kinetic Modeling, J. Phys. Chem. C. 121 (2017) 22644–22655. doi:10.1021/acs.jpcc.7b06524.

[52] V. Kotov, P.M.J. Koelman, Plug flow reactor model of the plasma chemical conversion of CO_2, Plasma Sources Sci. Technol. 28 (2019) 095002. doi:10.1088/1361-6595/ab3774.

[53] E.C. Neyts, K. Ostrikov, M.K. Sunkara, A. Bogaerts, Plasma catalysis: Synergistic

effects at the nanoscale, Chem. Rev. 115 (2015) 13408–13446. doi:10.1021/acs.chemrev.5b00362.

[54] A. Bogaerts, X. Tu, J.C. Whitehead, G. Centi, L. Lefferts, O. Guaitella, F. Azzolina-Jury, H.-H. Kim, A.B. Murphy, W.F. Schneider, T. Nozaki, J.C. Hicks, A. Rousseau, F. Thevenet, A. Khacef, M. Carreon, The 2020 plasma catalysis roadmap, J. Phys. D. Appl. Phys. In press (2020).

Supplementary material of:

How gas flow design can influence the performance of a DBD plasma reactor for dry reforming of methane.

Y. Uytdenhouwen [a,b], J. Hereijgers [c], T. Breugelmans [c], P. Cool [b], A. Bogaerts [a*]

[a] Research Group PLASMANT, Department of Chemistry, University of Antwerp, Universiteitsplein 1, Wilrijk B-2610, Belgium

[b] Research group LADCA, Department of Chemistry, University of Antwerp, Universiteitsplein 1, Wilrijk B-2610, Belgium

[c] Research group Applied Electrochemistry & Catalysis, University of Antwerp, Universiteitsplein 1, Wilrijk B-2610, Belgium

*Corresponding author:
Annemie Bogaerts
Universiteitsplein 1, B2.09
Wilrijk B-2610, Belgium
+3232652377
annemie.bogaerts@uantwerpen.be

1 Raw data of Figures 3 to 7

Table SI 1: Measured concentration of different calibrated components after the DRM reaction for all configurations used and plotted in Figure 3 to Figure 7. All components are measured on the TCD with the $H_2 : CO$ ratio shown in the last column.

Group	Configuration	CO₂ (%)	CH₄ (%)	H₂ (%)	O₂ (%)	CO (%)	Ethene (%)	Ethane (%)	Propane (%)	Ethanol (ppm)	H₂ : CO
One inlet – one outlet	L / 100 (i – iv)	43.1 ± 0.2	41.3 ± 0.8	6.0 ± 0.6	0.04 ± 0.01	6.4 ± 0.2	0.094 ± 0.005	0.97 ± 0.04	0.16 ± 0.03	66 ± 7	0.94
	S	44 ± 1	42 ± 1	6.4 ± 0.7	0.03 ± 0.01	7.2 ± 0.3	0.092 ± 0.005	1.03 ± 0.05	0.18 ± 0.03	108 ± 7	0.90
	75 (i)	43.2 ± 0.8	42 ± 1	5.9 ± 0.6	0.03 ± 0.01	6.3 ± 0.3	0.086 ± 0.007	0.9 ± 0.07	0.14 ± 0.02	94 ± 3	0.93
	50 (i)	44.1 ± 0.3	41.7 ± 0.7	5.7 ± 0.6	0.04 ± 0.01	5.9 ± 0.1	0.088 ± 0.006	0.91 ± 0.04	0.17 ± 0.03	84 ± 6	0.97
	25 (i)	45.1 ± 0.2	43.2 ± 0.8	5.0 ± 0.6	0.03 ± 0.02	5.15 ± 0.09	0.077 ± 0.007	0.83 ± 0.04	0.16 ± 0.02	83 ± 5	0.97
	75 (ii)	44.9 ± 0.2	45.5 ± 0.8	3.8 ± 0.2	0.006 ± 0.003	4.8 ± 0.3	0.069 ± 0.003	0.72 ± 0.02	0.11 ± 0.01	90 ± 3	0.79
	50 (ii)	46.2 ± 0.6	46.8 ± 1	2.6 ± 0.2	0.006 ± 0.003	3.8 ± 0.2	0.053 ± 0.002	0.52 ± 0.02	0.08 ± 0.02	85 ± 3	0.70
	25 (ii)	47.0 ± 0.3	49.0 ± 0.5	1.6 ± 0.2	0.002 ± 0.001	2.04 ± 0.05	0.0297 ± 0.0002	0.309 ± 0.008	0.047 ± 0.004	46 ± 4	0.77
	75 (iii)	48.4 ± 0.5	46.9 ± 0.6	3.6 ± 0.1	0.0096 ± 0.0006	5.0 ± 0.1	0.093 ± 0.006	0.81 ± 0.05	0.12 ± 0.02	140 ± 3	0.72
	50 (iii)	51.0 ± 0.1	48.1 ± 0.6	2.3 ± 0.4	0.010 ± 0.009	3.0 ± 0.4	0.085 ± 0.006	0.60 ± 0.04	0.08 ± 0.01	108 ± 4	0.78
	25 (iii)	51.0 ± 0.4	49.0 ± 0.4	1.4 ± 0.02	0.0073 ± 0.0004	1.99 ± 0.08	0.086 ± 0.004	0.44 ± 0.03	0.05 ± 0.01	72 ± 2	0.70
	75 (iv)	42.7 ± 0.7	40.6 ± 0.8	7.3 ± 0.7	0.03 ± 0.02	7.8 ± 0.2	0.089 ± 0.006	1.11 ± 0.05	0.18 ± 0.01	140 ± 20	0.93
	50 (iv)	40 ± 1	37.2 ± 1.0	9.6 ± 0.7	0.03 ± 0.01	10.5 ± 0.3	0.088 ± 0.006	1.37 ± 0.04	0.28 ± 0.02	111 ± 7	0.91
	25 (iv)	36.9 ± 0.8	31.9 ± 0.5	14 ± 1	0.04 ± 0.02	14.1 ± 0.4	0.080 ± 0.005	1.70 ± 0.06	0.37 ± 0.03	124 ± 3	0.99
CO₂ : CH₄ ratio	1:0	93 ± 1			2.10 ± 0.02	4.20 ± 0.07					
	6:1	73.9 ± 0.5	10.4 ± 0.2	5.1 ± 0.6	0.04 ± 0.02	9.06 ± 0.10		0.26 ± 0.01	0.012 ± 0.003		0.56
	3:1	64.0 ± 0.5	19.7 ± 0.3	5.6 ± 0.6	0.04 ± 0.02	8.8 ± 0.1	0.06 ± 0.006	0.44 ± 0.04	0.027 ± 0.003	25 ± 2	0.63
	1:1	43.1 ± 0.2	41.3 ± 0.8	6.0 ± 0.6	0.04 ± 0.01	6.4 ± 0.2	0.094 ± 0.005	0.97 ± 0.04	0.16 ± 0.03	66 ± 7	0.94
	1:3	22.6 ± 0.1	64 ± 1	6.1 ± 0.6	0.03 ± 0.02	3.13 ± 0.06	0.131 ± 0.007	1.31 ± 0.05	0.31 ± 0.04	64 ± 2	1.95
	1:6	13.2 ± 0.4	75 ± 3	5.7 ± 0.7	0.03 ± 0.01	1.68 ± 0.07	0.15 ± 0.01	1.37 ± 0.08	0.35 ± 0.02	38 ± 6	3.40
	0:1		90 ± 2	5.0 ± 0.1			0.208 ± 0.008	1.57 ± 0.04	0.42 ± 0.02	59 ± 10	
Residence time (s)	2.5	51.7 ± 0.4	48 ± 1	0.64 ± 0.02	0.0135 ± 0.0009	0.87 ± 0.02	0.069 ± 0.002	0.20 ± 0.01	0.017 ± 0.001	31 ± 1	0.74
	10	48.8 ± 0.2	46 ± 1	2.68 ± 0.04	0.014 ± 0.001	3.61 ± 0.06	0.096 ± 0.006	0.65 ± 0.04	0.11 ± 0.02	116 ± 6	0.74
	17.5	46.5 ± 0.4	43 ± 1	4.8 ± 0.1	0.013 ± 0.001	6.2 ± 0.2	0.094 ± 0.007	0.99 ± 0.06	0.15 ± 0.02	167 ± 9	0.77
	25	44.6 ± 0.2	40.0 ± 0.8	6.6 ± 0.2	0.011 ± 0.003	8.4 ± 0.2	0.095 ± 0.006	1.24 ± 0.04	0.20 ± 0.01	160 ± 10	0.79
	32.5	42.4 ± 0.3	37.8 ± 0.5	8.5 ± 0.2	0.016 ± 0.001	10.5 ± 0.3	0.096 ± 0.007	1.51 ± 0.06	0.26 ± 0.03	239 ± 9	0.81
	40	40.9 ± 0.4	36.2 ± 0.7	9.9 ± 0.2	0.015 ± 0.002	12.1 ± 0.3	0.093 ± 0.008	1.6 ± 0.06	0.29 ± 0.03	219 ± 5	0.82
	47.5	39.5 ± 0.2	34.5 ± 0.9	11.3 ± 0.2	0.013 ± 0.004	13.6 ± 0.5	0.095 ± 0.007	1.73 ± 0.05	0.33 ± 0.02	212 ± 2	0.83
	55	40 ± 1	30 ± 4	11 ± 2	0.010 ± 0.004	13 ± 2	0.097 ± 0.006	1.83 ± 0.05	0.35 ± 0.02	262 ± 5	0.87
	62.5	36.0 ± 0.2	31.5 ± 0.7	13.9 ± 0.4	0.025 ± 0.002	17 ± 2	0.089 ± 0.005	1.84 ± 0.04	0.35 ± 0.01	231 ± 5	0.81
	70	35.4 ± 0.7	30.8 ± 0.7	14.9 ± 0.4	0.0525 ± 0.0009	17.4 ± 0.4	0.093 ± 0.006	1.87 ± 0.05	0.40 ± 0.02	268 ± 4	0.86
Gradual addition CO₂ main – CH₄ side	LGA	42.8 ± 0.2	41.0 ± 0.8	6.0 ± 0.6	0.04 ± 0.01	7.2 ± 0.2	0.076 ± 0.006	0.80 ± 0.04	0.12 ± 0.02	60 ± 6	0.83
	SGA	41.2 ± 0.9	38.5 ± 0.9	8.6 ± 0.7	0.04 ± 0.02	9.0 ± 0.2	0.095 ± 0.006	1.21 ± 0.05	0.24 ± 0.02	120 ± 4	0.95
	1	42.9 ± 0.8	41 ± 1	6.3 ± 0.6	0.04 ± 0.01	6.7 ± 0.2	0.092 ± 0.007	0.97 ± 0.06	0.16 ± 0.02	95 ± 6	0.94
	2	43.3 ± 0.7	41.5 ± 0.9	6.7 ± 0.6	0.03 ± 0.01	7.2 ± 0.1	0.098 ± 0.004	1.04 ± 0.03	0.17 ± 0.02	87 ± 6	0.92
	3	43.4 ± 0.2	41.5 ± 0.7	6.4 ± 0.6	0.03 ± 0.01	7.5 ± 0.2	0.091 ± 0.005	0.99 ± 0.04	0.16 ± 0.02	90 ± 6	0.86
	4	43.2 ± 0.3	41.7 ± 0.7	6.4 ± 0.6	0.03 ± 0.01	7.6 ± 0.2	0.086 ± 0.006	0.88 ± 0.04	0.15 ± 0.03	83 ± 5	0.84
	5	43.2 ± 0.2	42.0 ± 0.7	6.3 ± 0.6	0.04 ± 0.01	7.9 ± 0.2	0.079 ± 0.007	0.76 ± 0.04	0.10 ± 0.03	104 ± 9	0.80

	6	43.0 ± 0.3	42.7 ± 0.8	5.8 ± 0.5	0.03 ± 0.01	8.1 ± 0.1	0.071 ± 0.006	0.57 ± 0.04	0.06 ± 0.01	52 ± 4	0.72
	7	42.9 ± 0.2	43.0 ± 0.8	5.7 ± 0.6	0.03 ± 0.02	8.2 ± 0.2	0.068 ± 0.005	0.46 ± 0.04	0.046 ± 0.008	35 ± 3	0.69
Gradual addition CH$_4$ main – CO$_2$ side	LGA	42.1 ± 0.3	38.5 ± 0.7	8.3 ± 0.5	0.02 ± 0.01	8.2 ± 0.1	0.108 ± 0.007	1.36 ± 0.05	0.28 ± 0.03	128 ± 5	1.00
	SGA	42.1 ± 0.8	38.2 ± 1.0	8.6 ± 0.6	0.04 ± 0.01	8.2 ± 0.2	0.098 ± 0.007	1.27 ± 0.04	0.28 ± 0.03	122 ± 4	1.05
	1	42.6 ± 0.3	40.0 ± 0.7	7.7 ± 0.7	0.03 ± 0.02	8.3 ± 0.2	0.099 ± 0.007	1.19 ± 0.05	0.21 ± 0.03	118 ± 7	0.92
	2	42.4 ± 0.6	40 ± 1	7.9 ± 0.6	0.03 ± 0.02	8.7 ± 0.2	0.099 ± 0.006	1.25 ± 0.06	0.23 ± 0.03	118 ± 5	0.91
	3	42.3 ± 0.8	39.5 ± 0.7	8.2 ± 0.7	0.03 ± 0.02	8.6 ± 0.2	0.100 ± 0.007	1.26 ± 0.06	0.23 ± 0.02	132 ± 6	0.96
	4	43.0 ± 0.3	39.8 ± 0.8	8.3 ± 0.6	0.04 ± 0.01	8.2 ± 0.2	0.101 ± 0.007	1.27 ± 0.06	0.26 ± 0.04	124 ± 6	1.01
	5	43 ± 1	40.3 ± 0.8	8.0 ± 0.8	0.03 ± 0.02	7.7 ± 0.3	0.103 ± 0.006	1.24 ± 0.06	0.24 ± 0.04	114 ± 6	1.04
	6	43.3 ± 0.9	40 ± 1	8.3 ± 0.7	0.04 ± 0.01	7.6 ± 0.2	0.106 ± 0.006	1.33 ± 0.04	0.28 ± 0.03	105 ± 5	1.09
	7	43.7 ± 0.6	39.9 ± 0.9	7.8 ± 0.6	0.03 ± 0.02	7.17 ± 0.06	0.106 ± 0.007	1.32 ± 0.04	0.30 ± 0.03	108 ± 3	1.09
Separate activation	LSN	44.1 ± 0.2	40.9 ± 0.6	6.5 ± 0.7	0.03 ± 0.02	7.0 ± 0.2	0.084 ± 0.005	0.97 ± 0.05	0.16 ± 0.02	100 ± 10	0.94
	LSW	43.6 ± 0.7	41.2 ± 0.9	6.2 ± 0.6	0.02 ± 0.01	7.0 ± 0.3	0.088 ± 0.007	0.98 ± 0.07	0.17 ± 0.02	109 ± 10	0.89
	SSN	43.4 ± 0.7	40.8 ± 0.7	7.2 ± 0.7	0.04 ± 0.02	7.3 ± 0.1	0.093 ± 0.007	1.12 ± 0.08	0.20 ± 0.02	113 ± 3	1.00
	SSW	42.2 ± 1.0	40.1 ± 0.8	8.3 ± 0.6	0.04 ± 0.01	8.1 ± 0.3	0.091 ± 0.004	1.17 ± 0.03	0.21 ± 0.02	136 ± 9	1.03

Table SI 2: GC peak areas for different uncalibrated components after the DRM reaction for all configurations used and plotted in Figure 3 to Figure 7. All components are measured on the FID, unless stated otherwise, and rescaled per column as stated in the second row.

Category	Component	Propene (TCD)	C2	C3	Isobutane / Methanol	n-Butane	2-methyl Butane / 2-propanol / acetone	n-Pentane / Diethylether	1	2,2-Dimethyl butane / 1-Propanol	2-Methyl pentane	3-Methyl pentane	n-Hexane	2	3	Heptane(1) / 1-Butanol	Heptane(2) / Cyclohexane	Heptane(3)
	Configuration	x1E3	x1E2	x1E1	x1E1	x1E1	x1E1	x1E1	x1E0	x1E1	x1E1	x1E1	x1E1	x1E1	x1E1	x1E1	x1E1	x1E1
One inlet – one outlet	L / 100 (i – iv)	30 ± 10	4060 ± 50	7300 ± 200	1580 ± 60	2100 ± 80	1830 ± 70	290 ± 20	1500 ± 200	300 ± 40	130 ± 30	870 ± 50	100 ± 30	60 ± 20	300 ± 100		130 ± 50	130 ± 30
	S	26 ± 9	4300 ± 100	8400 ± 400	1980 ± 60	2300 ± 100	2130 ± 100	300 ± 10	1510 ± 50	500 ± 200	190 ± 10	1020 ± 40	105 ± 4	69 ± 6	750 ± 90		270 ± 60	210 ± 60
	75 (i)	20 ± 10	3990 ± 50	7400 ± 200	1750 ± 20	2080 ± 60	1900 ± 50	273 ± 10	1460 ± 50	290 ± 60	150 ± 20	910 ± 30	110 ± 10	80 ± 10	600 ± 300		180 ± 40	150 ± 40
	50 (i)	29 ± 10	3850 ± 60	8000 ± 300	1800 ± 50	2160 ± 80	2020 ± 70	290 ± 10	1400 ± 50	330 ± 90	210 ± 20	920 ± 30	101 ± 9	60 ± 10	1400 ± 300		260 ± 30	160 ± 30
	25 (i)	20 ± 10	3550 ± 30	7600 ± 200	1750 ± 50	2000 ± 50	1970 ± 60	280 ± 4	1420 ± 50	450 ± 20	168 ± 9	810 ± 30	100 ± 10	80 ± 10	340 ± 30	73 ± 9	160 ± 20	90 ± 10
	75 (ii)	16 ± 7	2800 ± 40	4800 ± 200	1280 ± 40	1360 ± 40	1270 ± 50	164 ± 7	1010 ± 60	300 ± 70	135 ± 9	720 ± 30	90 ± 10	60 ± 10	870 ± 20		173 ± 10	150 ± 20
	50 (ii)	23 ± 8	1980 ± 50	2800 ± 200	950 ± 30	790 ± 70	840 ± 40	105 ± 5	820 ± 40	110 ± 30	49 ± 6	420 ± 40	49 ± 6	30 ± 7	300 ± 100		90 ± 20	80 ± 20
	25 (ii)	12 ± 2	1150 ± 30	1800 ± 100	540 ± 40	530 ± 30	490 ± 30	64 ± 5	400 ± 30	40 ± 10	24 ± 2	280 ± 20		17 ± 3	49 ± 5	9 ± 2	25 ± 3	36 ± 3
	75 (iii)	30 ± 10	3130 ± 40	4580 ± 70	1580 ± 10	1330 ± 20	1350 ± 20	156 ± 3	1090 ± 60	230 ± 10		780 ± 20		41 ± 7	400 ± 100		110 ± 20	100 ± 20
	50 (iii)	19 ± 8	2420 ± 30	2900 ± 100	1140 ± 20	870 ± 30	910 ± 20	108 ± 7	840 ± 50	380 ± 60	60 ± 5	530 ± 60	60 ± 10	40 ± 10	980 ± 80		80 ± 10	66 ± 10
	25 (iii)	17 ± 6	1580 ± 20	1470 ± 40	679 ± 8	470 ± 10	462 ± 9	52 ± 2	380 ± 40	130 ± 20		290 ± 20		17 ± 4	260 ± 30		39 ± 2	27 ± 6
	75 (iv)	20 ± 10	4500 ± 500	9500 ± 500	2300 ± 100	2700 ± 200	2460 ± 70	360 ± 20	1910 ± 40	500 ± 100	180 ± 20	1130 ± 40	142 ± 5	105 ± 6	370 ± 40	68 ± 9	170 ± 20	130 ± 10
	50 (iv)	30 ± 10	5800 ± 40	14400 ± 400	3050 ± 50	4000 ± 100	3590 ± 90	550 ± 20	2370 ± 40	1000 ± 100	380 ± 40	1610 ± 40	191 ± 7	170 ± 10	1200 ± 300	320 ± 50	440 ± 60	280 ± 50
	25 (iv)	40 ± 10	6910 ± 30	19800 ± 300	4300 ± 100	5900 ± 200	4900 ± 200	800 ± 20	2900 ± 300	1700 ± 100	570 ± 30	1980 ± 70	220 ± 20	250 ± 50	1000 ± 100	410 ± 40	500 ± 50	220 ± 20
$CO_2 : CH_4$ ratio	1:0																	
	6:1	42 ± 5	524 ± 1	189 ± 7	170 ± 10	70 ± 10	120 ± 20		260 ± 70			60 ± 30			289 ± 8			
	3:1	30 ± 10	1550 ± 10	1180 ± 9	500 ± 20	297 ± 7	499 ± 6	57 ± 3	790 ± 40	60 ± 10		230 ± 20	30 ± 10	21 ± 9	270 ± 6			
	1:1	30 ± 10	4060 ± 50	7300 ± 200	1580 ± 60	2100 ± 80	1830 ± 70	290 ± 20	1500 ± 200	300 ± 40	130 ± 30	870 ± 50	100 ± 30	60 ± 20	300 ± 100		130 ± 50	130 ± 30
	1:3	30 ± 20	5970 ± 40	17000 ± 200	2670 ± 30	5860 ± 50	3230 ± 30	730 ± 10	1650 ± 100	780 ± 10	513 ± 6	1400 ± 20	230 ± 20	150 ± 20	690 ± 40	340 ± 10	480 ± 20	270 ± 30
	1:6	30 ± 10	6490 ± 30	21000 ± 200	3240 ± 40	7480 ± 80	3770 ± 60	903 ± 8	1450 ± 80	1050 ± 20	730 ± 20	1400 ± 20	260 ± 30	240 ± 60	700 ± 100	500 ± 40	680 ± 60	220 ± 30
	0:1	40 ± 10	6860 ± 40	24100 ± 200	3910 ± 60	9140 ± 60	4310 ± 20	1030 ± 9	2100 ± 100	1400 ± 40	1020 ± 40	1263 ± 9	340 ± 30	280 ± 40	380 ± 40	750 ± 60	1000 ± 100	180 ± 80
Residence time (s)	2.5	3 ± 1	820 ± 40	791 ± 2	369 ± 5	228 ± 2	245 ± 3	22 ± 2	133 ± 7			60 ± 6			110 ± 20			
	10	30 ± 10	2700 ± 10	3950 ± 50	1300 ± 30	1170 ± 10	1110 ± 10	108 ± 4	650 ± 20	260 ± 40		630 ± 10		31 ± 2	1000 ± 100		110 ± 20	77 ± 10
	17.5	23 ± 10	4110 ± 30	7600 ± 100	2210 ± 60	2140 ± 30	2130 ± 30	229 ± 5	1380 ± 60	420 ± 30	138 ± 8	1100 ± 50		90 ± 30	800 ± 100		191 ± 7	142 ± 9
	25	21 ± 9	5060 ± 20	10540 ± 90	2610 ± 90	2840 ± 30	2820 ± 30	315 ± 5	1690 ± 30	500 ± 100	178 ± 4	1320 ± 40	81 ± 9	84 ± 7	1500 ± 500		270 ± 10	200 ± 10
	32.5	30 ± 20	6090 ± 50	14100 ± 200	3690 ± 10	3850 ± 40	4148 ± 7	477 ± 5	2660 ± 40	850 ± 20	295 ± 8	1800 ± 70	138 ± 8	155 ± 8	1340 ± 40	260 ± 10	380 ± 10	270 ± 10
	40	30 ± 20	6510 ± 40	15500 ± 100	3760 ± 20	4220 ± 40	4430 ± 20	521 ± 6	2730 ± 20	880 ± 20	317 ± 5	1866 ± 8	138 ± 9	140 ± 2	700 ± 300	266 ± 8	386 ± 5	264 ± 10
	47.5	40 ± 10	6780 ± 10	16780 ± 20	3920 ± 20	4591 ± 5	4930 ± 10	591 ± 1	3070 ± 50	1020 ± 20	372 ± 4	2015 ± 5	170 ± 7	190 ± 10	1290 ± 50	310 ± 20	437 ± 3	310 ± 10
	55	30 ± 10	7280 ± 10	18300 ± 100	4370 ± 30	5030 ± 30	4910 ± 40	636 ± 5	3260 ± 10	1160 ± 20	380 ± 10	2196 ± 9	161 ± 8	225 ± 4	1130 ± 20	280 ± 10	440 ± 10	300 ± 20
	62.5	30 ± 10	7150 ± 30	18800 ± 200	4380 ± 50	5200 ± 60	5700 ± 50	698 ± 8	3490 ± 30	1340 ± 70	430 ± 20	2230 ± 20	190 ± 7	250 ± 10	770 ± 30	400 ± 20	520 ± 10	345 ± 3
	70	40 ± 10	7384 ± 8	20000 ± 100	4740 ± 90	5630 ± 60	6700 ± 30	765 ± 5	3700 ± 100	1450 ± 30	450 ± 20	2280 ± 30	203 ± 6	270 ± 30	1100 ± 100	410 ± 30	520 ± 20	340 ± 20

Group		C1	C2	C3	C4	C5	C6	C7	C8	C9	C10	C11	C12	C13	C14	C15	C16	C17
Gradual addition CO$_2$ main – CH$_4$ side	LGA	20 ± 10	3430 ± 20	5200 ± 200	1270 ± 40	1370 ± 40	1460 ± 20	209 ± 6	1430 ± 50		140 ± 10	700 ± 30	100 ± 20	60 ± 10	890 ± 90		170 ± 20	140 ± 20
	SGA	30 ± 10	5220 ± 10	12750 ± 90	2820 ± 20	3620 ± 30	3170 ± 20	496 ± 4	2160 ± 50	880 ± 40	360 ± 10	1433 ± 8	160 ± 10	120 ± 20	1760 ± 60		430 ± 20	250 ± 30
	1	30 ± 10	4240 ± 40	8100 ± 100	1780 ± 30	2320 ± 30	2020 ± 30	316 ± 6	1680 ± 60	600 ± 200	220 ± 20	1040 ± 30	150 ± 20	100 ± 20	1100 ± 200		270 ± 30	230 ± 30
	2	36 ± 10	4390 ± 30	8270 ± 70	1820 ± 40	2340 ± 20	2050 ± 20	317 ± 7	1710 ± 50	300 ± 100	200 ± 20	1010 ± 20	140 ± 8	90 ± 8	1000 ± 100		250 ± 20	200 ± 20
	3	30 ± 10	4210 ± 20	7600 ± 100	1750 ± 30	2090 ± 20	1930 ± 20	283 ± 5	1620 ± 40	500 ± 100	200 ± 20	950 ± 20	126 ± 6	69 ± 8	1500 ± 200		270 ± 20	230 ± 10
	4	30 ± 10	3827 ± 7	6320 ± 40	1570 ± 40	1703 ± 7	1678 ± 9	230 ± 5	1470 ± 40		180 ± 10	828 ± 7	113 ± 6	59 ± 9	1400 ± 100		240 ± 10	200 ± 30
	5	20 ± 10	3360 ± 80	4600 ± 100	1500 ± 100	1280 ± 40	1390 ± 30	186 ± 6	1320 ± 60	211 ± 10	90 ± 20	600 ± 20	80 ± 10	34 ± 6	200 ± 100		80 ± 40	80 ± 20
	6	13 ± 9	2610 ± 30	2760 ± 30	950 ± 50	710 ± 10	896 ± 5	125 ± 3	1000 ± 50	103 ± 3	150 ± 60	390 ± 20	70 ± 20	27 ± 7	600 ± 300		80 ± 40	70 ± 30
	7	30 ± 10	1990 ± 20	1660 ± 50	680 ± 30	414 ± 5	610 ± 10	93 ± 5	830 ± 60		130 ± 30	270 ± 20	70 ± 10	24 ± 4	1000 ± 200			80 ± 20
Gradual addition CH$_4$ main – CO$_2$ side	LGA	30 ± 10	5730 ± 40	15200 ± 200	3230 ± 40	4550 ± 50	3630 ± 50	630 ± 10	2260 ± 90	930 ± 30	430 ± 20	1620 ± 30	200 ± 10	180 ± 20	780 ± 40	260 ± 20	400 ± 20	250 ± 20
	SGA	30 ± 10	5440 ± 90	14800 ± 400	3200 ± 100	4400 ± 100	3590 ± 100	620 ± 20	2270 ± 90	1040 ± 50	470 ± 20	1580 ± 40	190 ± 20	180 ± 30	1200 ± 200	350 ± 40	480 ± 40	280 ± 40
	1	30 ± 10	5060 ± 30	11220 ± 100	2490 ± 30	3160 ± 20	2760 ± 10	416 ± 5	1910 ± 50	600 ± 100	280 ± 10	1310 ± 10	150 ± 10	100 ± 10	1400 ± 100		350 ± 20	250 ± 30
	2	30 ± 10	5310 ± 90	12000 ± 300	2600 ± 60	3420 ± 80	2940 ± 50	470 ± 10	2080 ± 70	640 ± 30	300 ± 10	1370 ± 20	170 ± 10	130 ± 10	800 ± 200	170 ± 20	310 ± 20	220 ± 10
	3	30 ± 10	5480 ± 70	13000 ± 200	2840 ± 40	3730 ± 40	3170 ± 40	506 ± 8	2130 ± 60	720 ± 30	330 ± 10	1450 ± 20	170 ± 10	130 ± 10	800 ± 200	190 ± 20	320 ± 20	220 ± 20
	4	30 ± 10	5440 ± 90	13600 ± 400	2900 ± 90	3960 ± 100	3250 ± 80	540 ± 20	2200 ± 100	880 ± 50	390 ± 20	1500 ± 40	190 ± 20	140 ± 30	1600 ± 200		450 ± 30	300 ± 30
	5	30 ± 10	5300 ± 100	12900 ± 600	2700 ± 100	3800 ± 200	3100 ± 200	520 ± 30	2100 ± 100	790 ± 80	350 ± 40	1410 ± 70	180 ± 20	140 ± 20	1100 ± 400	240 ± 70	380 ± 60	260 ± 50
	6	30 ± 10	5640 ± 60	14800 ± 300	3010 ± 60	4500 ± 100	3430 ± 80	620 ± 10	2160 ± 50	1000 ± 100	440 ± 20	1530 ± 30	190 ± 20	160 ± 20	1400 ± 500	330 ± 60	440 ± 50	280 ± 30
	7	40 ± 10	5600 ± 90	15200 ± 300	3110 ± 80	4640 ± 90	3470 ± 60	640 ± 20	2090 ± 100	900 ± 200	500 ± 20	1550 ± 30	190 ± 30	120 ± 50	1800 ± 400	430 ± 40	530 ± 40	330 ± 30
Separate activation	LSN	16 ± 9	4240 ± 80	8600 ± 200	1960 ± 80	2380 ± 60	2150 ± 60	302 ± 9	1520 ± 60	470 ± 30	190 ± 10	1000 ± 30	105 ± 9	80 ± 10	600 ± 200	99 ± 3	180 ± 30	130 ± 10
	LSW	30 ± 10	4190 ± 100	8300 ± 300	1950 ± 70	2310 ± 60	2100 ± 50	296 ± 8	1530 ± 40	360 ± 90	190 ± 20	990 ± 10	120 ± 10	80 ± 20	1000 ± 600	80 ± 10	220 ± 50	170 ± 40
	SSN	30 ± 10	4700 ± 200	10300 ± 800	2300 ± 100	2900 ± 300	2500 ± 200	390 ± 40	1700 ± 100	560 ± 70	230 ± 30	1150 ± 90	140 ± 10	110 ± 10	470 ± 80	140 ± 30	220 ± 40	150 ± 30
	SSW	20 ± 10	5000 ± 100	11700 ± 500	2680 ± 70	3400 ± 200	3000 ± 200	460 ± 20	1980 ± 50	710 ± 40	270 ± 20	1270 ± 40	150 ± 20	130 ± 20	700 ± 100	190 ± 50	280 ± 30	170 ± 20

Table SI 3: Total mole equivalent FID peak area based on the number of C atoms per molecule (second column). and the individual shares of each component (third to last column). for the components formed during DRM for all configurations.

Component		Mole equivalent area (x 1E4)	C2	C3	Isobutane	n-Butane	2-methyl Butane	n-Pentane	2,2-Dimethyl butane	2-Methyl pentane	3-Methyl pentane	n-Hexane	Heptane(1)	Heptane(2) / Cyclohexane	Heptane(3)
One inlet – one outlet	L / 100 (i – iv)	24.32	0.83	0.10	0.02	0.02	0.02	0.0023	0.002	0.001	0.006	0.0007	0.0004	0.001	0.0008
	S	26.35	0.82	0.11	0.02	0.02	0.02	0.0022	0.003	0.001	0.006	0.0007		0.001	0.0011
	75 (i)	24.09	0.83	0.10	0.02	0.02	0.02	0.0023	0.002	0.001	0.006	0.0008	0.0004	0.001	0.0009
	50 (i)	23.70	0.81	0.11	0.02	0.02	0.02	0.0024	0.002	0.001	0.006	0.0007		0.002	0.0010
	25 (i)	21.96	0.81	0.12	0.02	0.02	0.02	0.0025	0.003	0.001	0.006	0.0008	0.0005	0.001	0.0006
	75 (ii)	16.80	0.83	0.09	0.02	0.02	0.02	0.0019	0.003	0.001	0.007	0.0009		0.001	0.0013
	50 (ii)	11.57	0.86	0.08	0.02	0.02	0.01	0.0018	0.002	0.001	0.006	0.0007		0.001	0.0010
	25 (ii)	6.80	0.85	0.09	0.02	0.02	0.01	0.0019	0.001	0.001	0.007	0.0005	0.0002	0.001	0.0008
	75 (iii)	18.43	0.85	0.08	0.02	0.02	0.01	0.0017	0.002	0.000	0.007	0.0005	0.0002	0.001	0.0008
	50 (iii)	13.96	0.87	0.07	0.02	0.02	0.01	0.0015	0.005	0.001	0.006	0.0007		0.001	0.0007
	25 (iii)	8.84	0.89	0.06	0.02	0.01	0.01	0.0012	0.002		0.006			0.001	0.0004
	75 (iv)	27.99	0.81	0.11	0.02	0.02	0.02	0.0026	0.003	0.001	0.007	0.0008	0.0003	0.001	0.0007
	50 (iv)	37.04	0.78	0.13	0.02	0.03	0.02	0.0030	0.005	0.002	0.007	0.0009	0.0012	0.002	0.0011
	25 (iv)	45.71	0.76	0.14	0.02	0.03	0.02	0.0035	0.006	0.002	0.007	0.0008	0.0013	0.002	0.0007
CO₂ : CH₄ ratio	1:0														
	6:1	2.80	0.94	0.02	0.02	0.01	0.01	0.0004			0.004		0.0076		
	3:1	8.51	0.91	0.05	0.01	0.01	0.01	0.0013	0.001		0.004	0.0006		0.001	0.0005
	1:1	24.32	0.83	0.10	0.02	0.02	0.02	0.0023	0.002	0.001	0.006	0.0007	0.0004	0.001	0.0008
	1:3	39.10	0.76	0.14	0.02	0.04	0.02	0.0037	0.003	0.002	0.006	0.0010	0.0012	0.002	0.0010
	1:6	43.82	0.74	0.16	0.02	0.04	0.02	0.0041	0.004	0.003	0.005	0.0010	0.0016	0.002	0.0007
	0:1	47.60	0.72	0.17	0.02	0.05	0.02	0.0043	0.005	0.004	0.004	0.0012	0.0022	0.003	0.0005
Residence time (s)	2.5	4.59	0.90	0.06	0.02	0.01	0.01	0.0009			0.002				
	10	15.84	0.85	0.08	0.02	0.02	0.01	0.0014	0.003		0.007			0.001	0.0007
	17.5	24.97	0.82	0.10	0.02	0.02	0.02	0.0018	0.003	0.001	0.007			0.001	0.0008
	25	31.24	0.81	0.11	0.02	0.02	0.02	0.0020	0.003	0.001	0.007	0.0004		0.001	0.0009
	32.5	38.58	0.79	0.12	0.02	0.02	0.02	0.0025	0.004	0.001	0.008	0.0006	0.0010	0.001	0.0010

	40	41.35	0.79	0.12	0.02	0.03	0.02	0.0025	0.004	0.001	0.008	0.0006	0.0009	0.001	0.0009
	47.5	43.49	0.78	0.13	0.02	0.03	0.02	0.0027	0.004	0.001	0.008	0.0007	0.0010	0.001	0.0010
	55	46.74	0.78	0.13	0.02	0.03	0.02	0.0027	0.004	0.001	0.008	0.0006	0.0009	0.001	0.0009
	62.5	46.56	0.77	0.13	0.02	0.03	0.02	0.0030	0.005	0.002	0.008	0.0007	0.0012	0.002	0.0011
	70	48.57	0.76	0.14	0.02	0.03	0.03	0.0031	0.005	0.002	0.008	0.0007	0.0012	0.002	0.0010
Gradual addition CO_2 main – CH_4 side	LGA	20.13	0.85	0.09	0.02	0.02	0.01	0.0021	0.002	0.001	0.006	0.0008		0.001	0.0010
	SGA	33.24	0.78	0.13	0.02	0.03	0.02	0.0030	0.004	0.002	0.007	0.0008		0.002	0.0011
	1	25.80	0.82	0.10	0.02	0.02	0.02	0.0025	0.004	0.001	0.007	0.0009		0.001	0.0013
	2	26.56	0.83	0.10	0.02	0.02	0.02	0.0024	0.002	0.001	0.006	0.0009		0.001	0.0011
	3	25.33	0.83	0.10	0.02	0.02	0.02	0.0022	0.003	0.001	0.006	0.0008		0.002	0.0013
	4	22.69	0.84	0.09	0.02	0.02	0.01	0.0020		0.001	0.006	0.0008		0.001	0.0013
	5	19.55	0.86	0.08	0.02	0.02	0.01	0.0019	0.002	0.001	0.005	0.0007		0.001	0.0006
	6	14.72	0.89	0.06	0.02	0.01	0.01	0.0017	0.001	0.002	0.004	0.0008		0.001	0.0007
	7	11.00	0.90	0.05	0.02	0.01	0.01	0.0017		0.002	0.004	0.0010		0.001	0.0010
Gradual addition CH_4 main – CO_2 side	LGA	37.19	0.77	0.14	0.02	0.03	0.02	0.0034	0.004	0.002	0.007	0.0009	0.0010	0.002	0.0010
	SGA	35.57	0.76	0.14	0.02	0.03	0.02	0.0035	0.005	0.002	0.007	0.0009	0.0014	0.002	0.0011
	1	31.57	0.80	0.12	0.02	0.03	0.02	0.0026	0.003	0.001	0.007	0.0008		0.002	0.0011
	2	33.23	0.80	0.12	0.02	0.03	0.02	0.0028	0.003	0.001	0.007	0.0009	0.0007	0.001	0.0010
	3	34.64	0.79	0.13	0.02	0.03	0.02	0.0029	0.003	0.002	0.007	0.0008	0.0008	0.001	0.0009
	4	34.82	0.78	0.13	0.02	0.03	0.02	0.0031	0.004	0.002	0.007	0.0009	0.0013	0.002	0.0012
	5	33.94	0.79	0.13	0.02	0.03	0.02	0.0030	0.004	0.002	0.007	0.0009	0.0010	0.002	0.0011
	6	36.49	0.77	0.14	0.02	0.03	0.02	0.0034	0.005	0.002	0.007	0.0009	0.0013	0.002	0.0011
	7	36.53	0.77	0.14	0.02	0.03	0.02	0.0035	0.004	0.002	0.007	0.0009	0.0017	0.002	0.0013
Separate activation	LSN	26.00	0.82	0.11	0.02	0.02	0.02	0.0023	0.003	0.001	0.006	0.0007	0.0005	0.001	0.0007
	LSW	25.57	0.82	0.11	0.02	0.02	0.02	0.0023	0.002	0.001	0.006	0.0008	0.0004	0.001	0.0009
	SSN	29.24	0.80	0.12	0.02	0.03	0.02	0.0027	0.003	0.001	0.007	0.0008	0.0007	0.001	0.0007
	SSW	31.59	0.79	0.12	0.02	0.03	0.02	0.0029	0.004	0.001	0.007	0.0008	0.0008	0.001	0.0008

Table SI 4: Conversions and energy cost, i.e. the energy needed to convert one mole of reactant mixture, shown for all configurations.

	Configuration	X_{CO_2}	X_{CH_4}	X_{total}	EC (kWh/mol)
One inlet – one outlet	L / 100 (i – iv)	12.9 ± 0.6	14.6 ± 0.7	13.7 ± 0.7	1.63 ± 0.04
	S	14.4 ± 0.5	15.5 ± 0.5	14.9 ± 0.5	1.50 ± 0.03
	75 (i)	13.2 ± 1.0	13.6 ± 0.9	13.4 ± 0.9	1.67 ± 0.10
	50 (i)	11.4 ± 0.8	14.4 ± 0.8	12.9 ± 0.8	1.7 ± 0.1
	25 (i)	10.4 ± 0.5	12 ± 1	11.2 ± 0.8	2.0 ± 0.1
	75 (ii)	9.1 ± 0.9	10 ± 2	10 ± 1	2.3 ± 0.2
	50 (ii)	6.5 ± 1.0	8 ± 1	7 ± 1	3.2 ± 0.4
	25 (ii)	2 ± 1	6 ± 1	4 ± 1	5.6 ± 0.6
	75 (iii)	9.5 ± 1.0	10 ± 1	10 ± 1	1.74 ± 0.08
	50 (iii)	4.6 ± 0.5	8 ± 1	6.1 ± 0.9	1.8 ± 0.2
	25 (iii)	4 ± 1	4 ± 2	4 ± 1	1.41 ± 0.09
	75 (iv)	15.2 ± 1.0	18 ± 2	16 ± 1	1.8 ± 0.1
	50 (iv)	20.1 ± 0.8	23.6 ± 1	21.9 ± 0.9	2.05 ± 0.01
	25 (iv)	26 ± 1	34.2 ± 0.8	30 ± 1	2.96 ± 0.09
CO_2 : CH_4 ratio	1:0	6 ± 2		6 ± 2	3.6 ± 0.9
	6:1	13 ± 1	24.5 ± 0.6	18.6 ± 0.9	1.5 ± 0.1
	3:1	14 ± 2	18 ± 3	16 ± 2	1.5 ± 0.2
	1:1	12.9 ± 0.6	14.6 ± 0.7	13.7 ± 0.7	1.63 ± 0.04
	1:3	8.6 ± 0.4	11.8 ± 0.4	10.2 ± 0.4	2.03 ± 0.05
	1:6	6.3 ± 0.5	9.8 ± 0.3	8.0 ± 0.4	2.42 ± 0.07
	0:1		7.3 ± 0.5	7.3 ± 0.5	3.1 ± 0.2
Residence time (s)	2.5	0.80 ± 0.07	2.8 ± 0.4	1.8 ± 0.3	1.5 ± 0.2
	10	6.7 ± 0.8	8 ± 4	7 ± 2	1.5 ± 0.4
	17.5	11 ± 1	13 ± 4	12 ± 3	1.5 ± 0.4
	25	13.4 ± 0.6	20 ± 3	17 ± 2	1.6 ± 0.2
	32.5	18 ± 1	24 ± 2	21 ± 1	1.66 ± 0.09
	40	21 ± 1	27 ± 3	24 ± 2	1.8 ± 0.1
	47.5	23.4 ± 0.8	31 ± 3	27 ± 2	1.9 ± 0.1
	55	22.9 ± 0.3	30 ± 2	27 ± 1	2.20 ± 0.09
	62.5	30.1 ± 0.6	37 ± 3	33 ± 2	2.0 ± 0.1
	70	31 ± 2	38 ± 3	35 ± 3	2.2 ± 0.1
Gradual addition CO_2 main – CH_4 side	LGA	12.6 ± 0.5	15.8 ± 0.2	14.2 ± 0.3	1.58 ± 0.02
	SGA	17 ± 1	21.0 ± 0.4	19.2 ± 0.8	1.17 ± 0.02
	1	12.4 ± 0.4	16.1 ± 0.4	14.2 ± 0.4	1.57 ± 0.02
	2	15 ± 1	16 ± 1	15 ± 1	1.47 ± 0.03
	3	14.5 ± 0.5	15.9 ± 0.4	15.2 ± 0.5	1.48 ± 0.04
	4	14.8 ± 0.5	15.5 ± 0.5	15.2 ± 0.5	1.48 ± 0.03
	5	15.5 ± 0.6	14.8 ± 0.1	15.1 ± 0.3	1.48 ± 0.01
	6	15.9 ± 0.7	13.4 ± 1.0	14.6 ± 0.9	1.53 ± 0.08
	7	16.0 ± 0.4	12.9 ± 0.2	14.5 ± 0.3	1.549 ± 0.007
Gradual addition	LGA	15.6 ± 0.8	20.9 ± 0.7	18.3 ± 0.8	1.23 ± 0.05
	SGA	16 ± 1	21.5 ± 0.8	19 ± 1	1.21 ± 0.06
	1	15.5 ± 0.7	19.7 ± 0.6	17.6 ± 0.7	1.27 ± 0.05

9

	2	16 ± 0.5	20.5 ± 0.4	18.2 ± 0.4	1.23 ± 0.02
	3	16 ± 1	21 ± 2	18 ± 1	1.21 ± 0.08
	4	16.1 ± 0.6	20.1 ± 0.7	18.1 ± 0.6	1.23 ± 0.04
	5	16 ± 2	19 ± 2	17 ± 2	1.3 ± 0.1
	6	15.6 ± 0.8	20 ± 3	18 ± 2	1.26 ± 0.09
	7	14.4 ± 0.8	19 ± 2	17 ± 1	1.34 ± 0.05
Separate activation	LSN	11.9 ± 0.5	17.6 ± 0.6	14.7 ± 0.5	1.52 ± 0.02
	LSW	12.7 ± 0.6	16 ± 2	14 ± 1	1.6 ± 0.1
	SSN	15 ± 1	17 ± 2	16 ± 1	1.41 ± 0.07
	SSW	16.5 ± 0.5	19 ± 2	18 ± 1	1.26 ± 0.06

2   Residence time distribution (RTD) simulations and measurements

2.1   Principle

Fluid flow through a reactor is rarely ideal, such as plug flow or mixed flow [19]. The geometry of the reactor, laminar or turbulent flow, diffusion, agitation, recirculation, stagnant regions, and shortcuts will influence the contact time in the reactor, resulting in a certain residence time distribution (RTD) instead of a fixed reaction time for all molecules. This RTD can be determined via a pulse experiment, i.e. adding a pulse of a tracer element to the inlet of the reactor, and recording the concentration of the tracer at the outlet as a function of time, giving us the age distribution curve, or E-curve. The shape of the E-curve can provide useful information about the flow in the reactor and can be used to calculate an average value for the residence time ($\bar{t}$) according to:

$$\bar{t} = \frac{\int_0^\infty tCdt}{\int_0^\infty Cdt} \cong \frac{\sum_i t_i C_i \Delta t_i}{\sum_i C_i \Delta t_i} \qquad (S1)$$

with C the trace concentration and t the time.

2.2   Highlights of the simulations

2.2.1   Model

CFD simulations were performed in COMSOL Multiphysics to determine a more theoretical RTD, in order to understand the changes seen in Figure 6 of the main text. A combined 'Laminar Flow' model and 'Transport of Diluted Species' model was used to simulate the convection (stationary) and diffusion (time dependent), respectively. A simplified model of the reactor was used (see Figure SI 1(b and d)), to determine the exact RTD of the reaction volume and omit the extra pathways of the inlet and outlet, next to the complete 2D geometry of the reactor (see Figure SI 1(a and c)).
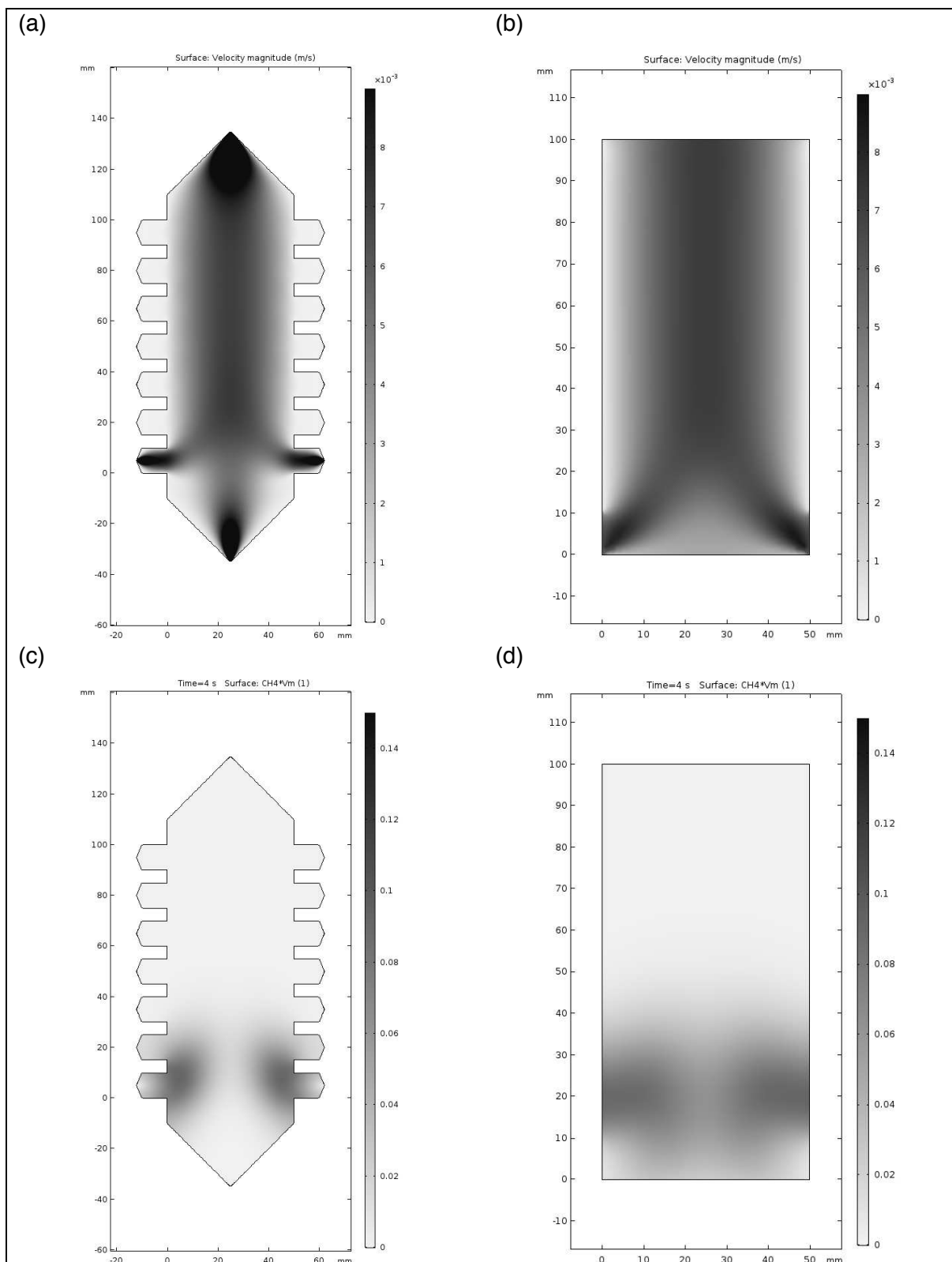
Figure SI 1: (a and b) Velocity profile and (c and d) example of a concentration profile of CH₄, (a and c) in the complete geometry of the reactor and (b and d) the simplified version.

Table SI 6 shows snapshots (with 1 second interval) of the RTD simulation from the separate addition configuration with CO_2 as the main gas and CH_4 added via entrance 1, see section 3.2.2 of the main text. The outlet concentration is measured at the upper border.

Table SI 5: Snapshots at different time steps of an example RTD CFD simulation.

13

t=16s	t=18s	t=20s	t=22s

t=24s	t=26s	t=28s	t=30s
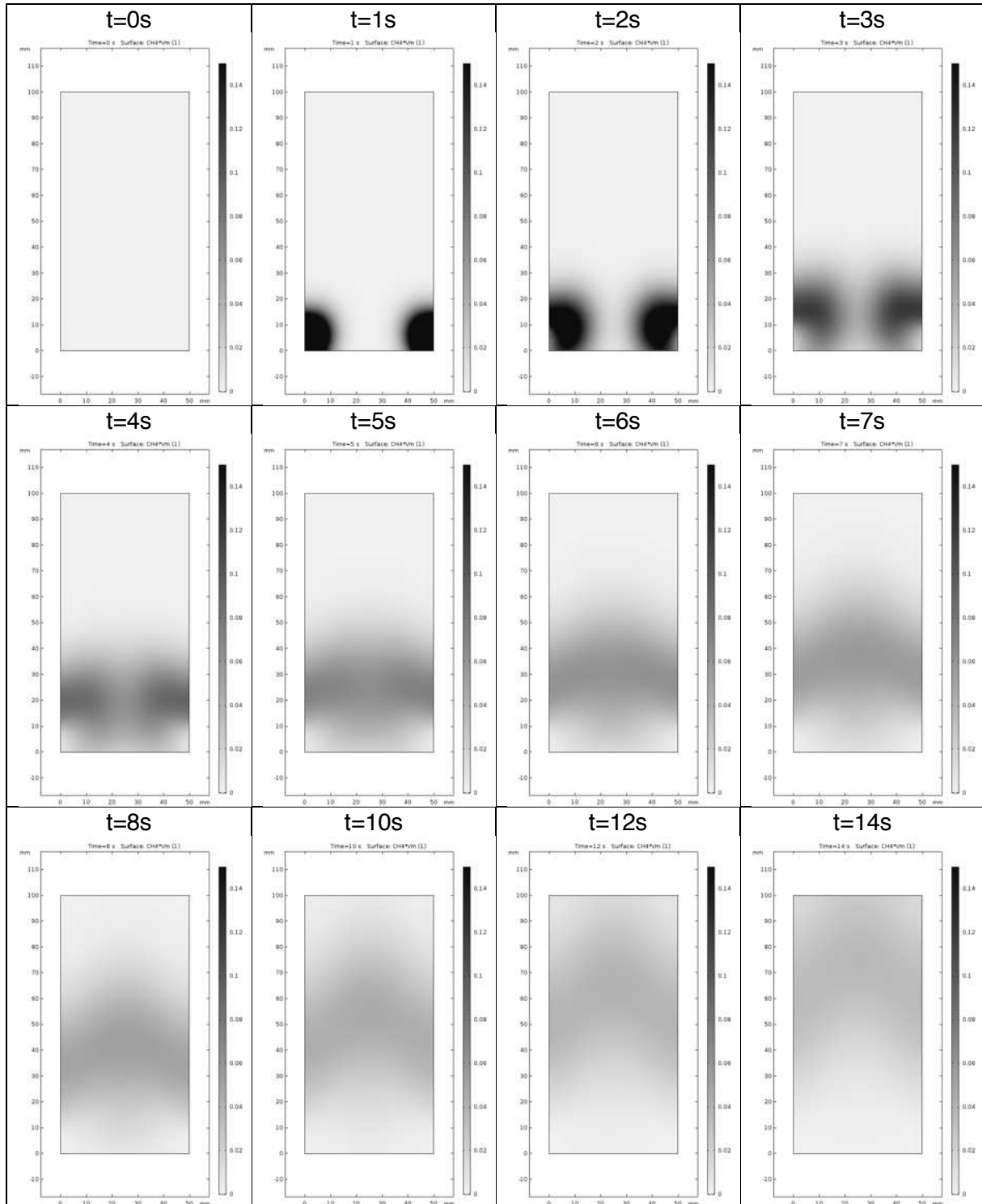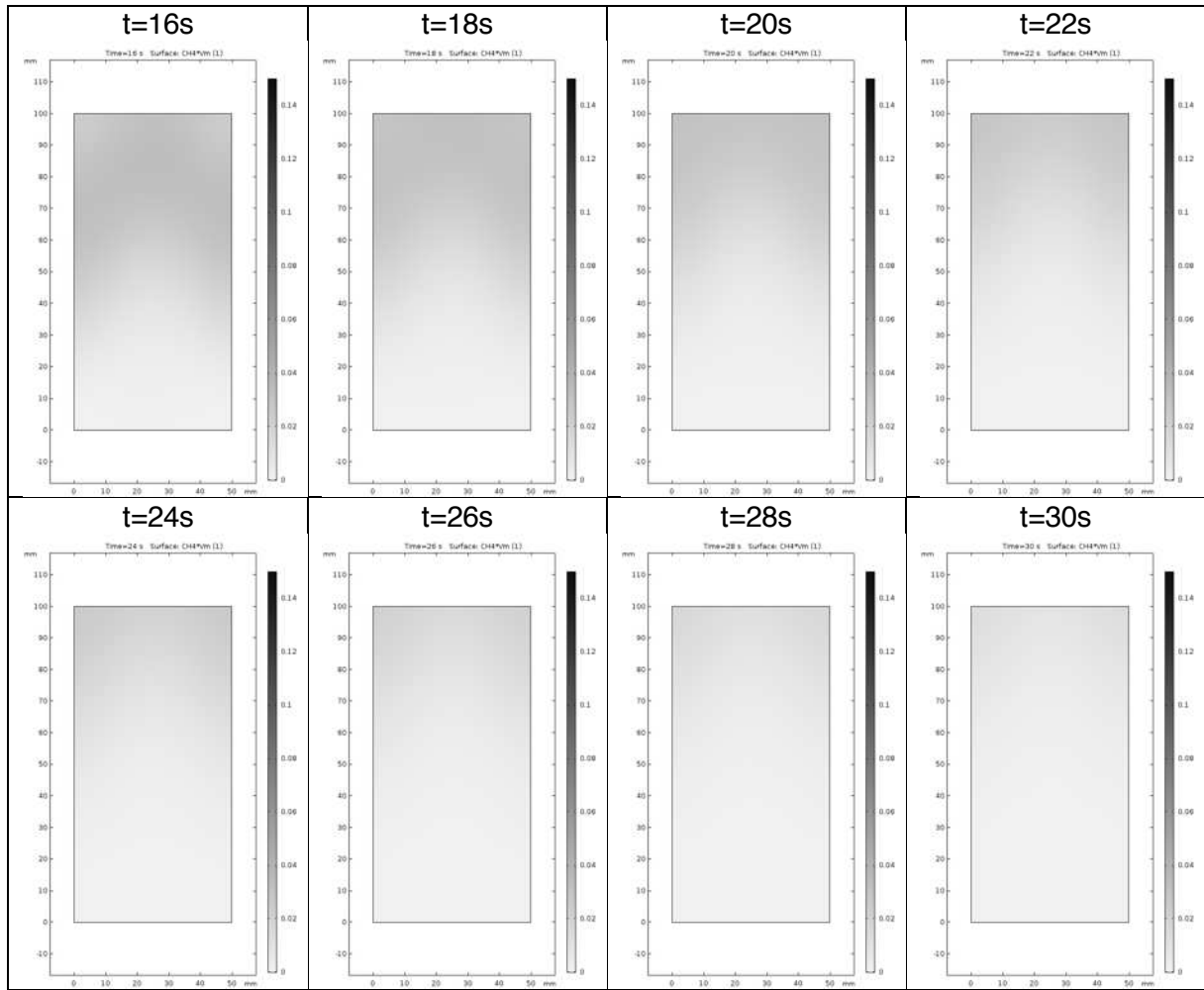
2.3   Results of the RTD study

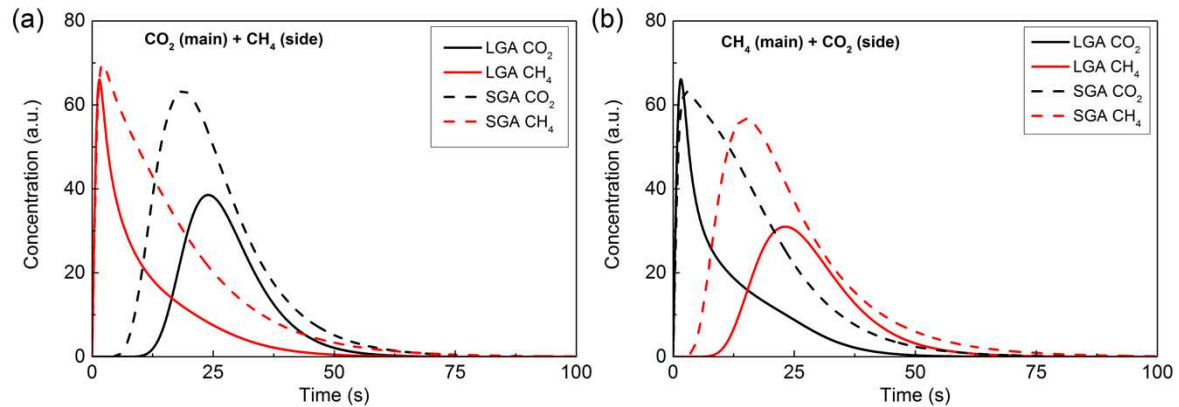### 2.3.1   Gradual addition
CFD results

Figure SI 2: Calculated RTD of CO_2 and CH_4 in the gradual addition configurations for (a) CO_2 as the main gas and (b) CH_4 as the main gas. The average calculated residence times can be found in Table SI 6.
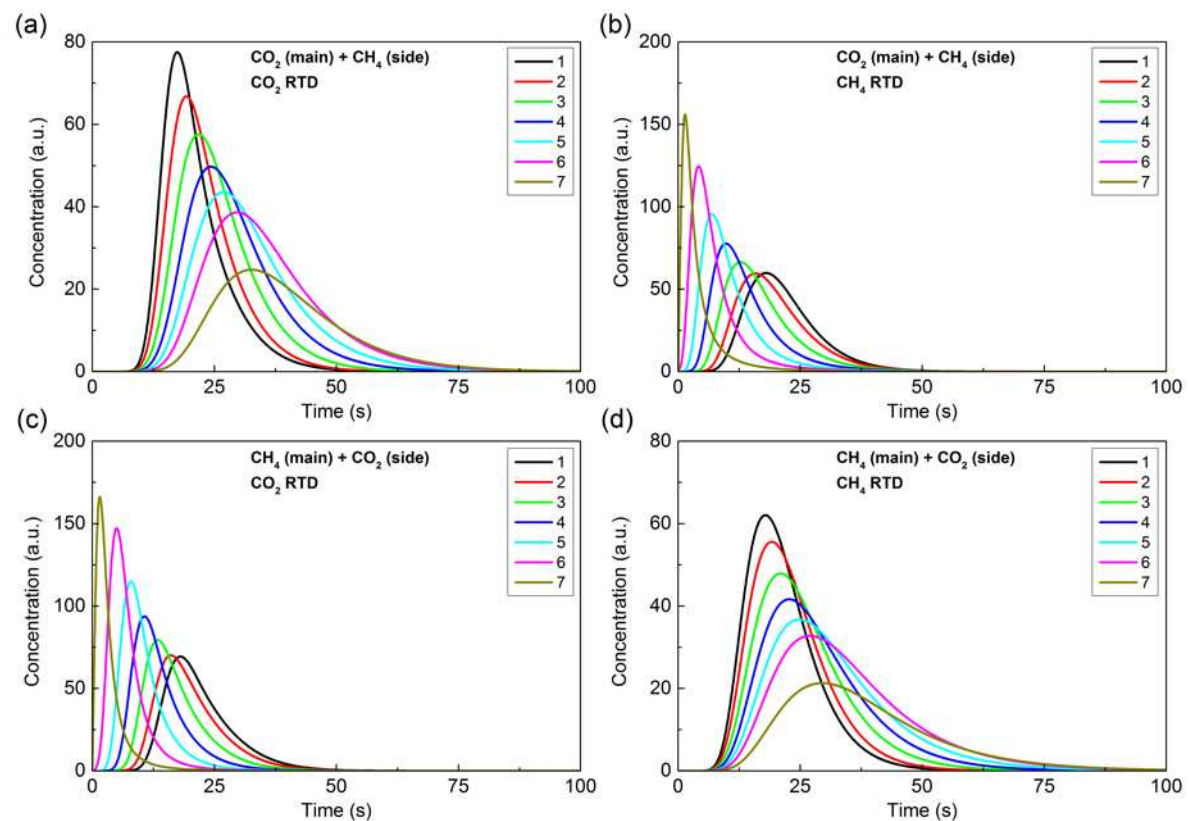
2.3.2   Separate addition
CFD results

Figure SI 3: Calculated RTD of (a and c) CO_2 and (b and d) CH_4 in the seperate addition configurations, for (a and b) CO_2 as the main gas and (c and d) CH_4 as the main gas, plotted for the different inlet pairs. The average calculated residence times can be found in Table SI 6.
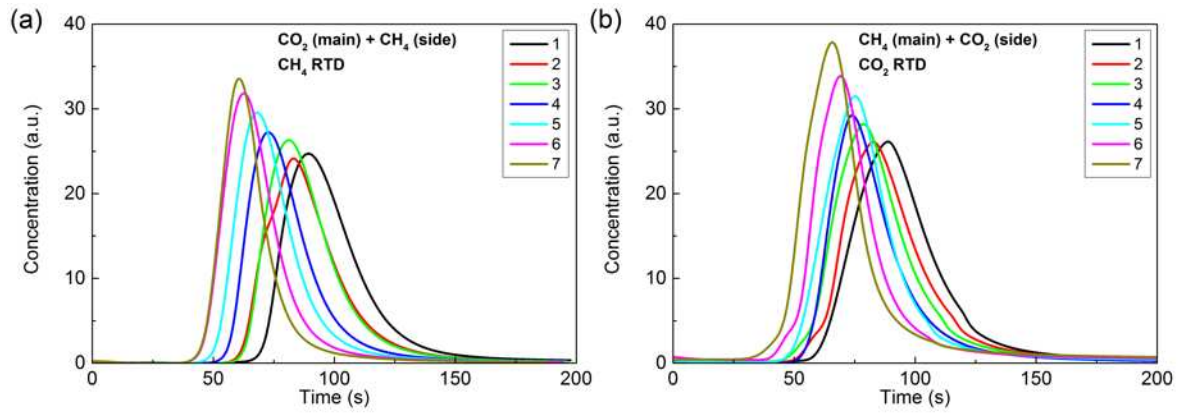
Experimental results

15

Figure SI 4: Experimental RTD of the added gas in the seperate addition configurations for (a) CO_2 as the main gas and (b) CH_4 as the main gas, plotted for the different inlet pairs. The average calculated residence times can be found in Table SI 6.
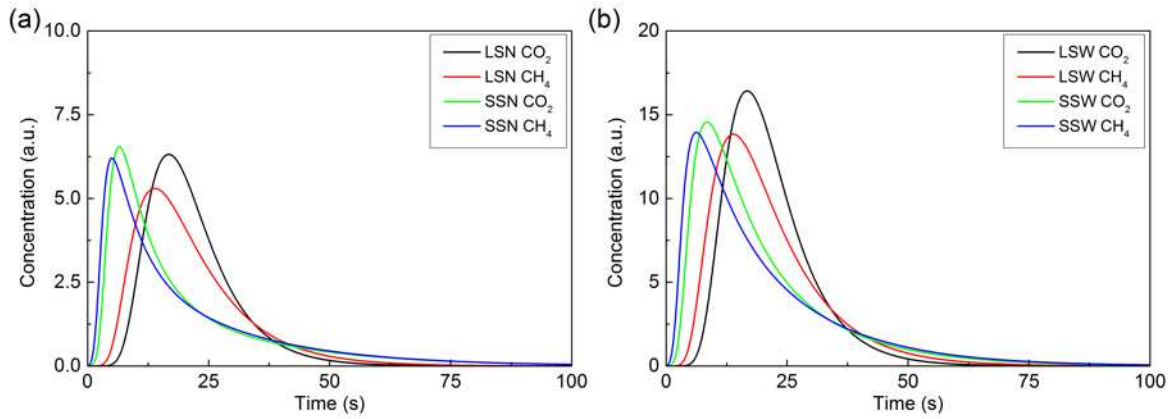
2.3.3 Separate pre-activation
CFD results

Figure SI 5: Calculated RTD of CO_2 and CH_4 in the pre-activation configurations. The average calculated residence times can be found in Table SI 6.

16

2.4 Summary of the obtained RTD data

Table SI 6: Calculated average residence times of the CFD simulations and experiments. Note that only the gradual addition cases were experimentally obtained due to their deviant behaviour in the main text of the manuscript. Also, only the added gas was pulsed in each case.

	Configuration	CFD		Experimental	
		CO_2 (s)	CH_4 (s)	CO_2 (s)	CH_4 (s)
Gradual addition CO_2 main – CH_4 side	LGA	28.0	11.2		
	SGA	25.2	16.1		
	1	21.1	21.6		99.1
	2	22.9	19.9		90.9
	3	25.9	17.1		89.8
	4	29.0	14.0		81.5
	5	32.3	10.9		76.2
	6	35.7	7.7		69.5
	7	39.1	4.4		66.7
Gradual addition CH_4 main – CO_2 side	LGA	11.4	28.2		
	SGA	15.4	24.2		
	1	22.0	21.5	100.2	
	2	20.1	23.0	95.8	
	3	17.1	25.7	91.5	
	4	13.9	28.6	85.8	
	5	10.6	31.7	87.2	
	6	7.2	34.8	83.8	
	7	3.6	37.9	80.8	
Separate activation	LSN	21.5	21.3		
	LSW	21.5	21.3		
	SSN	20.0	20.0		
	SSW	19.9	19.9		